

1 **Circadian protein regulation in the green lineage I. A phospho-dawn of**
2 **protein modification anticipates light onset in the picoeukaryote *O. tauri***

3
4 **Running title: Algal phospho- and protein rhythms**

5
6 **Zeenat B. Noordally^{1,2*}, Matthew M. Hindle^{1*}, Sarah F. Martin^{1,3}, Daniel D. Seaton^{1,4},**
7 **T. Ian Simpson⁵, Thierry Le Bihan^{1**}, Andrew J. Millar^{1**}**

8
9 ¹SynthSys and School of Biological Sciences, University of Edinburgh, Edinburgh EH9 3BF,
10 UK. ⁵Institute for Adaptive and Neural Computation, School of Informatics, University of
11 Edinburgh, Edinburgh EH8 9AB, UK.

12 * These authors contributed equally to this work.

13 ** corresponding authors: tlebihan@gmail.com; andrew.millar@ed.ac.uk +44 131 651 3325

14
15 ² Present address: Norfolk County Council, Community and Environmental Services, County
16 Hall, Martineau Lane, Norwich NR1 2DH, United Kingdom.

17 ³ Present address: Office of the Chief Statistician and Strategic Analysis, Scottish
18 Government, Edinburgh EH1 3DG, UK

19 ⁴ Present address: GlaxoSmithKline, Stevenage SG1 2NY, UK

20
21 Author; Email, ORCID:

22 Zeenat Noordally; zeenat.noordallyed@gmail.com, 0000-0003-2817-1330

23 Matthew Hindle; matthew.hindle@gmail.com, 0000-0002-6870-4069

24 Sarah F. Martin; sarahfriedemartin@gmail.com, -

25 Daniel Seaton; daniel.d.seaton@gmail.com, 0000-0002-5222-3893

26 Ian Simpson; Ian.Simpson@ed.ac.uk, 0000-0003-0495-7187

27 Thierry Lebihan; tlebihan@gmail.com, 0000-0003-0498-8063

28 Andrew Millar; andrew.millar@ed.ac.uk, 0000-0003-1756-3654

29 URL <https://www.ed.ac.uk/biology/centre-engineering-biology>

30
31 Submitted 13 December 2022; Main text: ~5000 words, excluding Methods 2730 words; 5
32 figures; 11 Supplementary Figures; 6 Supplementary Tables.

33	Table of Contents	
34	Highlight (<30 words)	3
35	Abstract (<200 words)	3
36	Keywords and Abbreviations.....	3
37	Introduction.....	4
38	Materials and Methods (2730 words)	6
39	Results.....	11
40	Diel rhythmicity of the transcriptome, proteome and phosphoproteome.....	11
41	Daytime peaks of protein abundance	13
42	Unusual, night-time proteins suggest a ‘dark state’	13
43	A phospho-dawn of protein modification	14
44	Functions of proteins with rhythmic phospho-motifs	15
45	Phase-specific target sites.....	15
46	Rhythmic regulation of the kinome.....	16
47	Discussion.....	16
48	The diel proteome and phosphoproteome	16
49	The ‘dark state’ is indirectly associated with lipid synthesis	17
50	Supplementary Data Summary	18
51	Acknowledgements.....	19
52	Author Contributions	19
53	Conflicts of Interest.....	19
54	Data Availability.....	19
55	REFERENCES	20
56	FIGURE LEGENDS	27
57	FIGURES	28
58	Supplementary Figure Legends	33
59	Supplementary Figures	35
60		
61		

62 Highlight (<30 words)

63 The phosphorylation of most protein sites was rhythmic under light-dark cycles, and
64 suggested circadian control by particular kinases. Day-peaking, rhythmic proteins likely
65 reflect light-stimulated protein synthesis in this microalga.

66 Abstract

67 Diel regulation of protein levels and protein modification had been less studied than transcript
68 rhythms. Here, we compare transcriptome data under light-dark cycles to partial proteome and
69 phosphoproteome data, assayed using shotgun mass-spectrometry, from the alga *Ostreococcus*
70 *tauri*, the smallest free-living eukaryote. 10% of quantified proteins but two-thirds of
71 phosphoproteins were rhythmic. Mathematical modelling showed that light-stimulated protein
72 synthesis can account for the observed clustering of protein peaks in the daytime. Prompted by
73 night-peaking and apparently dark-stable proteins, we also tested cultures under prolonged
74 darkness, where the proteome changed less than under the diel cycle. The dark-stable,
75 prasinophyte-specific proteins were also reported to accumulate when *O. tauri* formed lipid
76 droplets. In the phosphoproteome, 39% of rhythmic phospho-sites reached peak levels just
77 before dawn. This anticipatory phosphorylation suggests that a clock-regulated phospho-dawn
78 prepares green cells for daytime functions. Acid-directed and proline-directed protein
79 phosphorylation sites were regulated in antiphase, implicating the clock-related, casein kinases
80 1 and 2 in phase-specific regulation, alternating with the CMGC protein kinase family.
81 Understanding the dynamic phosphoprotein network should be facilitated by the minimal
82 kinome and proteome of *O. tauri*. The data are available from ProteomeXchange, with
83 identifiers PXD001734, PXD001735 and PXD002909. This submission updates a previous
84 version, posted on bioRxiv on 4th April 2018, as
85 <https://www.biorxiv.org/content/10.1101/287862v1>

86 Keywords and Abbreviations

87 **Keywords:** Systems biology; light signalling; proteomics; phosphoproteomics; photoperiod;
88 marine microalgae; photosynthetic pico-eukaryotes

89
90 **Abbreviations:** PM, phosphopeptide motif; LD, light-dark cycles; ZT, Zeitgeber Time; DA,
91 dark adaptation; PC, principal component; CK1, casein kinase 1; CK2, casein kinase 2;
92 GSK3, Glycogen Synthase Kinase 3; CMGC, Cyclin-dependent kinase, Mitogen-activated
93 protein kinase, Glycogen synthase kinase, CDC-like kinase; CCA1, Circadian Clock
94 Associated 1 protein.

95

96 Introduction

97 Responses to light are critical for organisms of the green lineage (Noordally and Millar,
98 2015; Paaanen *et al.*, 2021). The rapid effects of photosynthetic light harvesting, for example
99 on redox state and sugar metabolism, are complemented by signalling photoreceptors
100 (Whitelam and Halliday, 2007) and the slower, 24-hour regulation by the biological clock
101 (Millar, 2016; Creux and Harmer, 2019). Circadian regulation allows organisms to anticipate
102 the predictable, day-night transitions of the diel cycle, complementing the responses to faster
103 changes in light levels (Troein *et al.*, 2011). Mehta *et al.* (2021) refer to these as
104 ‘anticipatory’ and ‘reactive’ regulation. At the macromolecular level, the transcriptomes in
105 the green lineage show widespread and overlapping regulation of mRNA abundance by both
106 light and circadian signals (see below), whereas the diel regulation of proteins and their post-
107 translational modifications had been less studied (Mehta *et al.*, 2021). We addressed that gap
108 using a minimal biological system, focussing on protein phosphorylation.

109
110 Phosphorylation of an existing protein is energetically inexpensive, occurs rapidly and can
111 then alter protein activity through conformational change or intermolecular recognition
112 (Khoury *et al.*, 2011). These characteristics seem fitted to reactive regulation. Some plant
113 photoreceptor proteins include protein kinases that initiate light signalling (Christie, 2007;
114 Djouani-Tahri *et al.*, 2011a).

115
116 Protein synthesis is not only far slower but also among the costliest macromolecular
117 processes (Scott *et al.*, 2010; Karr *et al.*, 2012), seemingly more suited to anticipatory
118 regulation. Rhythmic regulation might then provide a selective advantage, loosely
119 summarised as making proteins when they are needed in the diel cycle (Laloum and
120 Robinson-Rechavi, 2022). That reasoning helped to interpret the co-regulation of functional
121 clusters of RNAs, when transcriptome studies demonstrated that over 50% of Arabidopsis
122 RNAs can be rhythmic under diel, light-dark cycles (LD) (Smith *et al.*, 2004; Blasing *et al.*,
123 2005; Michael *et al.*, 2008). Most strikingly, almost the whole transcriptome of the marine
124 unicellular alga *Ostreococcus tauri* was rhythmic in controlled conditions (Monnier *et al.*,
125 2010) and this was also the most-rhythmic taxon among the diverse plankton of a Pacific
126 timeseries (Kolody *et al.*, 2019). The clock might also allow anticipation, to ensure that the
127 proteins had been fully synthesised and assembled to their active state by the appropriate
128 time.

129
130 Proteomic data, in contrast, revealed that most detected proteins had stable levels, with an
131 average half-life >6 days in the model plant *Arabidopsis thaliana* (Li *et al.*, 2017), suggesting
132 little scope for diel rhythmicity. Timeseries under constant light or a diel cycle found up to
133 6% of rhythmic proteins (Baerenfaller *et al.*, 2012, 2015)(Choudhary *et al.*, 2016; Uhrig *et al.*,
134 2021; Krahmer *et al.*, 2022). The most short-lived, regulatory proteins are harder to
135 detect, but such proteins seem to be exceptions to the general protein stability, consistent with
136 mammalian systems (Doherty *et al.*, 2009). Global regulation of protein synthesis is also
137 clearly relevant in plants and algae (Piques *et al.*, 2009; Juntawong and Bailey-Serres, 2012;
138 Pal *et al.*, 2013; Misra *et al.*, 2015; Ishihara *et al.*, 2015). In this context, circadian RNA
139 regulation was proposed to offer a selective advantage through seasonal adaptation to day-
140 length on a timescale of weeks (Seaton *et al.*, 2018).

141
142 More protein phosphorylation sites change over the diel cycle, compared to protein levels
143 (Kusakina and Dodd, 2012; Mehta *et al.*, 2021). Protein phosphorylation in plants and algae
144 is most directly light-regulated by the photoreceptor kinases (Christie, 2007; Djouani-Tahri *et al.*
145 *et al.*, 2011a), though light also affects the broader phosphoproteome (Turkina *et al.*, 2006;

146 Boex-Fontvieille *et al.*, 2014; Schönberg *et al.*, 2017), for example affecting 25% of
147 Arabidopsis phosphopeptides within 30 minutes (Uhrig *et al.*, 2021). Circadian studies in
148 Arabidopsis under constant light found up to 23% rhythmic phosphopeptides (Choudhary *et*
149 *al.*, 2015; Kraemer *et al.*, 2022). These studies suggest that light responses and the circadian
150 clock in Arabidopsis each control five- to ten-fold more phosphopeptides than the diel
151 rhythm of total protein level, so it is also important to understand which phospho-regulators
152 mediate these effects.

153

154 The amino acid sequences of rhythmically-regulated phosphosites have implicated a range of
155 protein kinases with overlapping contributions in Arabidopsis (Choudhary *et al.*, 2015; Uhrig
156 *et al.*, 2021; Kraemer *et al.*, 2022). However, ~1000 protein kinases shape the
157 phosphoproteome in Arabidopsis (Champion *et al.*, 2004) including several in plastids
158 (Baginsky and Gruijsem, 2009), compared to half that number in the human genome
159 (Manning *et al.*, 2002). Of particular interest, the casein kinases (CK1, CK2) and Glycogen
160 Synthase Kinase 3 (GSK3), affect the circadian timing of all organisms suitably studied
161 (Mehra *et al.*, 2009). These kinases have central positions in the yeast kinase-target network
162 (Breitkreutz *et al.*, 2010) and are highly conserved (Hindle *et al.*, 2014), in contrast to
163 photoreceptor proteins or circadian transcription factors (Noordally and Millar, 2015; Dunlap
164 and Loros, 2017).

165

166 Here, we compare the prevalence of proteomic and phosphoproteomic regulation under LD
167 cycles, using *O. tauri* as a minimal model for the green lineage (Noordally and Millar, 2015).
168 This alga not only has a ubiquitously-rhythmic transcriptome, but its genome is also reduced
169 to 13Mbp (Blanc-Mathieu *et al.*, 2014), likely due to selection pressure to reduce cell size to
170 1-2µm (Courties *et al.*, 1994). Its 7699 protein-coding genes include just 133 protein kinases
171 that represent the core families for eukaryotic signalling (Hindle *et al.*, 2014) and a minimal
172 set of Arabidopsis clock gene homologues (Corellou *et al.*, 2009; Djouani-Tahri *et al.*,
173 2011b; Troein *et al.*, 2011; Ocone *et al.*, 2013). CK1 and CK2 modulate circadian timing in
174 the light, with widespread effects on the algal phosphoproteome (Le Bihan *et al.*, 2011, 2015;
175 van Ooijen *et al.*, 2013). A non-transcriptional, 24-hour oscillator of unknown mechanism
176 was also revealed under prolonged darkness, when transcription stops in this organism
177 (O'Neill *et al.*, 2011; van Ooijen *et al.*, 2011; Edgar *et al.*, 2012; Bouget *et al.*, 2014; Feeney
178 *et al.*, 2016). In cyanobacteria, the non-transcriptional clock is driven by rhythmic protein
179 phosphorylation, so rhythmic protein kinase activities could also be relevant in *O. tauri* (van
180 Ooijen and Millar, 2012; Wong and O'Neill, 2018).

181

182 Our results reveal widespread daily rhythms in both the proteome and phosphoproteome in *O.*
183 *tauri*, including expected features such as the diel control of conserved, cell cycle phospho-
184 regulators. Rather than rapid phosphorylation responses and slow, rhythmic anticipation in
185 protein profiles, however, the level of many rhythmic proteins appears light-responsive,
186 whereas much of the rhythmic phosphoproteome anticipates dawn. The phosphosite
187 sequences strongly implicate phase-specific protein kinase classes. Moreover, we identify a
188 set of rhythmic, algal-specific proteins that accumulate in prolonged darkness and were also
189 identified in conditions that promote the formation of lipid droplets.

190 Materials and Methods (2730 words)

191 Materials

192 Chemicals were purchased from Sigma-Aldrich (now a subsidiary of Merck Life Science UK
193 Ltd, Dorset, UK) unless otherwise stated. Main solvent, acetonitrile and water for liquid
194 chromatography– dual mass spectrometry (LC-MSMS) and sample preparation were HPLC
195 quality (Thermo Fisher Scientific, Loughborough, UK). Formic acid was Suprapure 98-100%
196 (Merck) and trifluoroacetic acid (TFA) was 99% purity sequencing grade. Porcine trypsin
197 TPCK treated was from Worthington (Lorne Laboratories, Reading, UK). All HPLC-MS
198 connectors and fittings were from Upchurch Scientific (Hichrom, Theale, UK) or Valco
199 (RESTEK, High Wycombe, UK). % are expressed in v/v.

201 *O. tauri* media and culturing

202 *Ostreococcus tauri* OTTH95 were cultured as previously described (van Ooijen *et al.*, 2012),
203 supplemented with 0.22 μm filtered 50 $\mu\text{g ml}^{-1}$ ampicillin, neomycin and kanamycin
204 antibiotics in vented tissue culture flasks (Sarstedt, Leicester, UK). Cultures were maintained
205 by splitting weekly at 1:50 dilution. In preparation for proteomics experiments, cultures were
206 grown in growth media supplemented with 200 mM sorbitol and 0.4% glycerol prior to
207 harvesting (O'Neill *et al.*, 2011). Cells were cultured under cycles of 12 hour light/ 12 hour
208 dark (LD) at 20°C in a controlled environment chamber (MLR-350, Sanyo Gallenkamp,
209 Loughborough, UK) at a light intensity of 17.5 $\mu\text{Em}^{-2} \text{s}^{-1}$ white fluorescent light filtered by
210 724 Ocean Blue filter (LEE Filters Worldwide, Andover, UK).

212 *O. tauri* cell harvesting

213 Cells were grown for 7 days in LD and on the seventh day harvested, with five replications,
214 at Zeitgeber Time (ZT) 0, 4, 8, 12, 16 and 20, where ZT0 corresponds to dawn. At ZT0 cells
215 were harvested a few minutes before the lights went on and at ZT12, before the lights went
216 off. 135 ml culture was harvested by centrifugation (4000 rpm, 10 min, 4°C) per sample
217 replicate, each from a separate culture vessel. Pellets were resuspended in ice cold phosphate
218 buffered saline solution (PBS). Cultures were centrifuged as before, pellets were air dried and
219 then vortex-mixed in 250 μl 8M urea and stored at -80°C. For total cell lysate, cells were
220 dissolved by sonication (Branson Ultrasonics) and diluted with 500 μl dH₂O.
221 Cells were grown for 7 days in LD and on the eighth day the Dark Adaptation (DA)
222 experiment cell harvests were performed at ZT24, 48, 72 and 96 in constant darkness with
223 five replications. The samples were harvested and prepared as for the LD experiment.

225 Protein digestion

226 Samples were analysed by Bradford Assay (Bio-Rad, Watford, UK) and 400 μg protein of
227 each sample was used in the digestion. Samples were reduced in 10 mM dithiothreitol and 50
228 mM ammonium bicarbonate, and alkylated with 25 mM iodoacetamide. Samples were
229 digested overnight with 10 μg (1:40 ratio) trypsin under agitation at room temperature at pH8
230 in a total volume of 1 ml. Samples were cleaned on SPE BondElut 25 mg columns (Agilent
231 Technologies, Stockport, UK) following the vendor instruction. 50 μl (~20 μg) was removed
232 and dried for LC-MS (Speedvac, Thermo Fisher Scientific). The remaining ~380 μg were
233 also dried in preparation for phosphopeptide enrichment, and stored at -20°C.

234

235 Phosphopeptide enrichment

236 Dried peptide samples (~380 µg) were sonicated in 50 µl solution 0 (2.5% acetonitrile, 0.5%
237 TFA) and 100 µl solution 2 (80% acetonitrile, 0.5% TFA, 100% lactic acid). Titansphere
238 Phos-TiO Kit spin tip-columns (GL Sciences, Tokyo, Japan) were washed with 40 µl solution
239 1 (80% acetonitrile, 0.5% TFA). Samples were loaded on the spin tip-columns and passaged
240 three times through a centrifuge; 5 min at 200 xg, 15 min incubation at room temperature and
241 10 min at 200 xg. Spin tip-columns were subsequently washed once with solution 1, twice
242 with solution 2 and twice with solution 1 for 2 min at 200x g. Phosphopeptides were eluted in
243 two steps, first with 50 µl 5% ammonium hydroxide (5 min at 200 xg) and secondly, with 5%
244 pyrrolidine solution. 20 µl 20% formic acid was added to lower the pH and samples were
245 cleaned on Bond Elut OMIX C18 pipette tips (Agilent Technologies) following the
246 manufacturer's instruction.

247

248 Protein and phosphoprotein quantification

249 15 µg protein from total *O. tauri* cell lysates were run on a Novex NuPAGE 4-12% Bis-Tris
250 by SDS-PAGE with PeppermintStick Phosphoprotein Molecular Weight Standards and
251 Spectra Multicolor Broad Range Protein Ladder (Thermo Fisher Scientific). The gel was
252 fixed overnight (50% methanol, 40% ddH₂O, 10% glacial acetic acid), washed in ddH₂O and
253 stained with Pro-Q Diamond Phosphoprotein Gel Stain (Invitrogen, now Thermo Fisher
254 Scientific, Loughborough, UK) in the dark at 25°C following manufacturer's instructions.
255 The gel was imaged on a Typhoon TRIO variable mode imager (GE Healthcare, Amersham,
256 UK) at 532 nm excitation/ 580 nm emission, 450 PMT and 50 micron resolution. Images
257 were processed using ImageQuant TL software (GE Healthcare, Amersham, UK). The gel
258 was re-used for protein quantification using SYPRO Ruby Protein Gel Stain (Thermo Fisher
259 Scientific, Loughborough, UK) following manufacturer's instructions and imaged using a UV
260 transilluminator (Ultra-Violet Products Ltd, Cambridge UK). Protein and phosphoprotein
261 bands were quantified using Image Studio Lite v 4.0 (LI-COR Biosciences, Cambridge, UK).

262

263 Protein per cell quantification

264 Cells were grown (as described above) and independent, triplicate cultures were harvested at
265 the times indicated. Cultures were monitored using spectrophotometry at 600nm. Total
266 protein was quantified using the Quick Start Bradford Assay following manufacturer
267 instructions (Bio-Rad, Watford, UK). Cell number was estimated either by counting four
268 fields of view per culture in a haemocytometer after trypan blue staining (Abcam protocols,
269 Cambridge, UK), or by fluorescence-activated cell sorting (FACS). For FACS, a 1/200
270 dilution of cells were transferred to fresh media containing 1X SYBR Green I Nucleic Acid
271 Gel Stain (Invitrogen, now Thermo Fisher Scientific, Loughborough, UK) and FACS-
272 counted (FACScan, BD Bioscience, Wokingham, UK) at a flow rate of 60µl per minute.

273

274 qPCR for transcriptional regulation during dark adaptation (DA)

275 Cells were cultured and harvested in the same experimental regime (described above) and
276 harvested in biological triplicate at the times indicated for the LD and DA experiments. Total
277 RNA was extracted from frozen cells using an RNeasy Plant Mini Kit and DNase treated
278 (QIAGEN, Manchester, UK). First-strand cDNA was synthesised using 1 µg RNA and 500
279 ng µl⁻¹ Oligo(dT)₁₅ primer (Promega, Southampton, UK), denatured at 65°C for 5 min, and
280 reverse transcribed using SuperScript II (Invitrogen, now Thermo Fisher Scientific,
281 Loughborough, UK) at 42 °C for 50 min and 70 °C for 10 min. 1/100 cDNA dilutions were
282 analysed using a LightCycler[®]480 and LightCycler[®]480 SYBR Green I Master (Roche,

283 Welwyn Garden City, UK) following manufacturer's instructions and cycling conditions of
284 pre-incubation 95°C for 5 min; 45x amplification cycles of 95°C for 10 s, 60°C for 10 s,
285 72°C for 10 s. The following 5' to 3' forward (F) and reverse (R) primers to *O. tauri* gene
286 loci were used: ostta01g01560 GTTGCCATCAACGGTTTCGG (F),
287 GATTGGTTCACGCACACGAC (R); ostta03g00220 AAGGCTGGTTTGGCACAGAT (F),
288 GCGCTTGCTCGACGTTAAC (R); ostta03g04500 GCCGCGGAAGATTCTTTCAAG (F),
289 TCATCCGCCGTGATGTTGTG (R); ostta04g02740 ATCACCTGAACGATCGTGCG (F),
290 CCGACTTACCCTCCTTAAGCG (R); ostta10g02780 GGCGTTCTTGGAATCTCTCGT
291 (F), TATCGTCGATGATCCCGCCC (R); ostta10g03200 GGTACGGAGGAAGAAGTGGC
292 (F), ATGTCCATGAGCTTCGGCAA (R); ostta14g00065 GACAGCCGGTGGATCAGAAG
293 (F), TCGAGGTAGCTCGGGAGATC (R); ostta16g01620 ACGGGTTGCAGCTCATCTAC
294 (F), CCGCTTGGGTCCAGTACTTC (R); ostta18g01250 CTTGCAAATGTCCACGACGG
295 (F), ATGATGTGGCACGTCTACC (R); OtCpg00010 ACATGACTCACGCGCCTTAA
296 (F), TGCCAAAGGTGCCCTACAAA (R). Primers to eukaryotic translation
297 elongation/initiation factor (EF1a) ostta04g05410 GACGCGACGGTGGATCAA (F) and
298 CGACTGCCATCGTTTTACC (R) were used as an endogenous control. Data were
299 combined for biological and two technical replicates and relative quantification performed
300 using LightCycler[®]480 1.5 software (Roche).

301

302 HPLC–MS analysis

303 Micro-HPLC-MS/MS analyses were performed using an on-line system consisting of a
304 micro-pump 1200 binary HPLC system (Agilent Technologies) coupled to an hybrid LTQ-
305 Orbitrap XL instrument (Thermo Fisher Scientific). The complete method has been described
306 previously (Le Bihan *et al.*, 2010). For all measurements, 8µl of sample was injected using a
307 micro-WPS auto sampler (Agilent Technologies) at 5µl /min. After sample loading, the flow
308 rate across the column was reduced to approximately 100-200 nl/min using a vented column
309 arrangement. Samples were analysed on a 140 min gradient for data dependant analysis.

310

311 HPLC-MS data analysis

312 To generate files compatible with public access databases PRIDE (Vizcaino *et al.*, 2016) and
313 the former pep2pro (Hirsch-Hoffmann *et al.*, 2012), Mascot Generic Format (MGF) input
314 files were generated using MSConvert from ProteoWizard (Kessner *et al.*, 2008). MSMS data
315 was searched using MASCOT version 2.4 (Matrix Science Ltd, London, UK) against the *O.*
316 *tauri* subset of the NCBI protein database (10114 sequences from NCBI version 2014 June
317 6th including common contaminants) using a maximum missed-cut value of 2, variable
318 oxidation (M), N-terminal protein acetylation, phosphorylation (STY) and fixed
319 carbamidomethylation (C); precursor mass tolerance was 7 ppm and MSMS tolerance 0.4
320 amu. The significance threshold (p) was set below 0.05 (MudPIT scoring). Global FDR was
321 evaluated using decoy database search and removal of peptides ranked higher than 1 for a
322 mascot score above 20 (~1% global FDR). Mass spectrometry proteomics data have been
323 deposited in PRIDE ProteomeXchange Consortium (Vizcaino *et al.*, 2014) via the PRIDE
324 partner repository with the dataset identifier LD global proteomics, PXD001735; LD
325 phosphoproteomics, PXD001734; DA global proteomics, PXD002909. Data was converted
326 into PRIDEXML using Pride converter 2.0.20 and submitted using proteome exchange tool
327 pxsubmission tool 2.0.1. The LC-MS data were also publicly available in the former pep2pro
328 database (Assemblies 'Ostreococcus tauri Light:dark cycle,LD global', 'Ostreococcus tauri
329 Light:dark cycle,LD phospho', and 'Ostreococcus tauri dark adaptation,DA global').
330 Label-free quantification was performed using Progenesis version 4.1 (Nonlinear Dynamics,
331 Newcastle, UK). Only MS peaks with a charge of 2+, 3+ or 4+ and the five most intense

332 spectra within each feature were included in the analysis. Peptide abundances were mean-
333 normalised and ArcSinH transformed to generate normal datasets. Within-group means were
334 calculated to determine fold changes. Neutral losses of phosphoric acid typical of serine and
335 threonine phosphorylated were validated manually in all significantly differential
336 phosphopeptides. Ambiguous sites were confirmed by cross-referencing (by sequence,
337 charge, and quantity of residue modifications) with most probable site predictions from
338 MaxQuant version 1.0.13.8 (Cox and Mann, 2008) in singlet mode, Mascot settings as above.
339 Where multiple occurrences of residue phosphorylation events were quantified, abundances
340 were summed, collating all charge states, missed cuts and further modifications.

341

342 Data analysis

343 Merging

344 For accurate and unique phosphopeptide quantification we addressed variant redundancy at
345 different charge states, alternative modifications (e.g. oxidation and acetylation) and multiple
346 sites of protease digestion. All unique phosphorylation events were retained, including
347 multiple phosphorylation, at a given amino acid motif, while summing the quantification of
348 these technical variants. The qpMerge (<http://sourceforge.net/projects/ppmerge/>) software
349 was used to combine Progenesis and MaxQuant phospho-site predictions and produce a
350 unique set of quantified phosphopeptide motifs (Hindle *et al.*, 2016).

351 Outlier identification and removal

352 To detect outliers we applied principal component analysis (PCA) of replicates and
353 comparing each replicates r^2 to the respective median abundance at that ZT. A single
354 replicate, 4E, was excluded based on extreme differences in peptide quantification as viewed
355 in the wider distribution of the ratios to the sample median, which was confirmed with a
356 Pearson's correlation against a defined criterion of a sample median of < 0.8 (Supplementary
357 Figures S1).

358 P-value calculation and false discovery rate (FDR)

359 For analysing the significance of changing protein and peptide abundance over time, non-
360 linear response of expression using polynomial regression was modelled using the R Stats
361 Package. A third order polynomial was fitted, allowing for an expected peak and trough
362 within a 24 h daily cycle. An arcsinh transformation of abundance was applied to meet the
363 required assumption of normality (Burbidge *et al.*, 1988). FDR was calculated using the
364 Benjamini and Hochberg (BH) method (Benjamini and Hochberg, 1995). More than 2
365 quantifying peptides were required to report protein abundance.

366 Equivalence testing

367 Using the R equivalence package, the statistical equivalence of mean abundance across time
368 was tested as the highest p -value from exhaustive pairwise Two one-sided test approach
369 (TOST) tests over all ZTs (Schuirmann, 1981; Westlake, 1981). We tested whether
370 abundances had upper and lower differences of less than 0.3 within the equivalence margin
371 (ϵ).

372 O. tauri gene identifiers

373 *O. tauri* genome version 1 gene IDs (Derelle *et al.*, 2006) for microarray data were converted
374 to version 2 IDs (Blanc-Mathieu *et al.*, 2014) by finding exact sequence matches for the
375 microarray probes (Accession GPL8644) (Monnier *et al.*, 2010) in the version 2 FASTA
376 coding sequence file.

377 Principle component analysis (PCA)

378 PCA was used to investigate the main components of variation in the data using prcomp from
379 the R Stats Package. The abundances were zero-centred per-feature. The PCA values for each
380 feature were extracted and then used for Gene Ontology (GO) enrichment analysis.

381 **Clustering**

382 Hierarchical clustering was performed with hclust from the R Stats Package and applied on
383 per-feature (protein or phosphopeptide motif) mean abundances over time, which were zero-
384 centred and scaled. Pearson's correlation was used to calculate distance matrix and the Ward
385 method (Ward, 1963) for linkage criteria. The hierarchical tree was divided into clusters
386 using the dynamicTreeCut algorithm (Langfelder *et al.*, 2008). The hybrid cut tree method
387 with a cut height of 100 and a minimum cluster size of 20 was used for both datasets.
388 Clusters are displayed with 95% (black lines) and 99% (orange lines) confidence via
389 multiscale bootstrap resampling (AU determined p-value).

390 **Enrichment analysis for GO terms**

391 TopGO was used to evaluate the enrichment of GO terms, for each ontology aspect, within
392 clusters, peaks, troughs, and principal components. For clusters, peaks and troughs a Fisher's
393 exact test was used by partitioning at 95% confidence on FDR corrected *p*-values, and with a
394 fold change >1.5 in normalised abundance. For each test, we use a relevant background of
395 non-significant observed features. To test for enrichment of GO terms for each PCA the
396 Kolmogorov-Smirnov test was applied over the absolute PCA values for each gene. GO
397 terms were predicted by InterProScan 5 (Jones *et al.*, 2014) on amino acids sequences for *O.*
398 *tauri* coding sequences (NCBI version 140606 (Blanc-Mathieu *et al.*, 2014)).

399 **Homology modelling**

400 Structural homology models were generated using I-TASSER (Yang and Zhang, 2015) for
401 prasinophyte-family specific proteins of unknown structure and function, including for
402 ostta02g03680 compared to the human Bar-domain protein structure in PDB entry with DOI
403 10.2210/pdb2d4c/pdb. Other suggested homologies were more limited.

404 **pLOGO and binomial statistics**

405 Significantly over- and under-represented amino acid residues at different time-points were
406 calculated using the binomial based pLogo tool (O'Shea *et al.*, 2013). The Motif-X tool
407 (Chou and Schwartz, 2011) was used to discover novel motifs in the dataset. Binomial
408 statistics were applied to calculate the enrichment of motifs and the combined probabilities of
409 amino acids with similar properties in a phospho-motif (*e.g.* the acidic D/E positions in the
410 CK2 motif).

411 **Kinase target prediction**

412 Computational prediction of protein kinase motifs associated with the identified
413 phosphorylation sites was performed using Group-based Prediction System, GPS Version 3.0
414 (<http://gps.biocuckoo.org/index.php>) (Xue *et al.*, 2011).

415 ***O. tauri* loci IDs mapping to *A. thaliana* loci IDs**

416 *O. tauri* and *A. thaliana* IDs were mapped using EggNOG4.1 (<http://eggnogdb.embl.de>). *O.*
417 *tauri* proteins were downloaded from
418 https://bioinformatics.psb.ugent.be/gdb/ostreococcusV2/LATEST/OsttaV2_PROT_20140522
419 .fasta.gz (May 22nd, 2014). Viridiplantae (virNOG) hmms and their descriptions and
420 annotations were transferred to *O. tauri* proteins using hmmer 3.1 (<http://hmmer.janelia.org>)
421

422 **Mathematical simulations**

423 **Simulated protein rhythms**

424 Protein dynamics ($P(t)$) were simulated according to the following model:

$$425 \quad \frac{dP(t)}{dt} = \left((k_{syn} - 1)L + 1 \right) m(t) - k_{deg}P(t)$$

426 Where $L(t) = 1$ during the day ($ZT \leq 12$), and 0 otherwise. The rate of protein degradation
427 (k_{deg}) was set to 0.1 h^{-1} , and the ratio of protein synthesis in the light compared to the dark
428 (k_{syn}) was set to 4, based on (Martin *et al.*, 2012). The rhythmically expressed mRNA levels
429 ($m(t)$) are given by:

430
$$m(t) = \cos\left(\frac{2\pi(t - \varphi)}{24}\right) + 1$$

431 The peak phase of expression is given by φ . To obtain the distributions of peak and trough
432 protein levels, the peak phases (φ) of mRNA expression were uniformly distributed at 0.1 h
433 intervals across the range [0,24]. For each phase of mRNA expression, the timing of peak and
434 trough protein levels was determined by simulating the model dynamics in MATLAB using
435 the ode15s ODE solver. The peaks and troughs were identified across a 24 h period,
436 following 240 h simulation to allow the dynamics to reach a steady behaviour (i.e. with the
437 same protein levels at ZT0 and ZT24).

438 **Protein degradation rates and depletion during dark adaptation**

439 Degradation rates were calculated from published proteomics data (Martin *et al.*, 2012),
440 which characterised the dynamics of partial ¹⁵N isotope incorporation. We assumed a
441 labelling efficiency of 0.93 (=maximum labelled fraction achieved of any protein + 0.01), and
442 fitted a simple kinetic model assuming: (1) constant labelling efficiency over time; (2)
443 different proteins are labelled at the same efficiency; (3) heavy and light fractions are turned
444 over at equal rates, similar to (Seaton *et al.*, 2018). One protein with a high degradation rate
445 ~0.03 h⁻¹ was excluded as an outlier, which increased the correlation from R = -0.48 to -0.7
446 when included.

447

448 **Results**

449

450 To understand the landscape of protein abundance and phosphorylation across the diel cycle,
451 we harvested quintuplicate biological samples of *O. tauri* at six timepoints across a 12 h
452 light/12 h dark (LD) cycle. Dawn samples (zeitgeber time 0, ZT0) were harvested just before
453 lights-on, and samples at ZT12 before lights-off, to detect biological regulation that
454 anticipated these transitions. The proteome and phosphoproteome were measured in whole-
455 cell extracts from each sample, by label-free, liquid chromatography–mass spectrometry
456 (Figure 1A). After removing a technical outlier (Supplementary Fig. S1), 855 proteins were
457 quantified with 2 or more peptides (Supplementary Table S1). Phosphopeptides were
458 enriched by metal-affinity chromatography prior to detection. For quantification, we
459 combined the phosphopeptide species that shared phosphorylation on a particular amino acid,
460 irrespective of other modifications (Hindle *et al.*, 2016). We refer to this set of
461 phosphorylated species as a phosphopeptide motif (PM). 1472 phosphopeptide motifs were
462 quantified, from 860 proteins (Supplementary Table 2). Serine and threonine residues were
463 modified most; only 1% of PMs included phospho-tyrosine. The quantified proteins and
464 phosphoproteins each represent ~11% of the total *O. tauri* proteome (Figure 1B). 29 out of 61
465 proteins encoded on the chloroplast genome (Robbens *et al.*, 2007) were quantified, with 6
466 PMs. 3 out of 43 mitochondrial-encoded proteins were quantified with no PMs, consistent
467 with other studies (Ito *et al.*, 2009).

468

469 **Diel rhythmicity of the transcriptome, proteome and phosphoproteome**

470 To compare the patterns and prevalence of daily rhythms at different regulatory levels, we re-
471 analysed published transcriptome data in parallel with these protein and phosphoprotein data,
472 summarised in Figure 1C. Gene expression in *O. tauri* was strongly rhythmic under LD
473 cycles, with 89% of transcripts scored rhythmic, as previously reported (Monnier *et al.*,
474 2010). 85 (9.5%) of the detected proteins were significantly rhythmic and changed by at least
475 1.5-fold, with only 11 of these proteins changing level by more than 5-fold. In contrast, 66%

476 of phosphoproteins or 58% of PMs (570 of 860 proteins; 850 of 1472 PMs) were rhythmic by
477 these criteria and the levels of 35 PMs changed more than 20-fold. The overlap among all
478 three datasets included only 110 genes. The most common pairwise overlaps involved genes
479 with changing levels of RNA and/or PMs but not of protein (Figure 1C).

480

481 Protein levels nonetheless changed smoothly, with distinct waveforms. Of the twenty most
482 highly-detected proteins, likely including the most abundant, 11 were significantly rhythmic
483 but with low amplitudes (Supplementary Figure S2A), such that only *ostta10g03200*
484 exceeded the 1.5-fold change threshold (Table S1). 15 of the twenty most highly-detected
485 PMs, in contrast, were rhythmic by both criteria (Supplementary Figure S2B). The more
486 stringent, “equivalence” test revealed 49 proteins with significantly non-changing protein
487 abundance but with significantly changing transcript and PMs, illustrated by the 10-fold
488 change in PM abundance on the non-changing, chlorophyll-binding protein CP26, amongst
489 others (Supplementary Figure S3).

490

491 To address our major question on the dominant patterns of regulation, we used undirected,
492 principal component (PC) analysis (Fig. 1D-1I). Clustering (Fig. 1D-1I, Supplementary
493 Figure S4) and analysis of peak distributions (Fig. 2A-C) informed more detailed hypotheses
494 on upstream regulation and downstream, functional effects. The PC analysis represented most
495 (83-86%) of the variance in the data sets but indicated a differing balance of molecular
496 regulation (Supplementary Table S3). The transcriptome and phosphoproteome data clearly
497 separated between dawn and dusk timepoints (in PC1), whereas the light and dark intervals
498 were separated by the secondary PC2. This mapped the 13 transcriptome and 6
499 phosphoproteome timepoints into their respective, temporal sequences. Gene Ontology (GO)
500 terms relating to translation, ribosome biogenesis and RNA processing were enriched among
501 dawn-expressed RNAs, and mitotic processes (DNA replication and repair) among dusk-
502 expressed transcripts (Supplementary Table S3), similar to past analysis (Monnier *et al.*,
503 2010). The functions of rhythmic phosphoproteins are discussed in more detail, below.

504

505 The regulation was strikingly reversed in the proteome (Fig. 1C, 1D), where the major
506 separation (in PC1) was between samples from light and dark intervals. The early day (ZT4),
507 when translation and chlorophyll biosynthesis GO terms were enriched, was separated from
508 all other timepoints, most strongly from mid-night (ZT16 and 20). There was less separation
509 (in PC2) of the late night (ZT0), when proteins involved in the TCA cycle and transport
510 processes are prominent, from the late day (ZT8-12), when translation and chlorophyll
511 biosynthesis were still enriched. In contrast, the ZT0 timepoint stood out in the
512 phosphoproteome (Fig. 1E, 1F), when PMs enriched for transcription, glucose metabolism,
513 K⁺ and protein transport and ubiquitin-dependent proteolysis functions were clearly separated
514 from the late-day timepoints (ZT8, ZT12). PC2 separated mid-day timepoints (ZT4, ZT8,
515 with enrichment for regulation of gene expression, translation and transmembrane transport)
516 from mid-night (ZT16, ZT20, when mitosis and Ca²⁺ transmembrane transport terms were
517 enriched).

518

519 The even distribution of changing RNAs across all the transcriptomic timepoints was not
520 reflected either in the proteome or the phosphoproteome data, where the early day (ZT4) or
521 pre-dawn (ZT0) timepoints, respectively, stood out in the PC analysis. Hierarchical clustering
522 grouped the protein and PM abundance profiles into 8 clusters (termed P1–P8 and PM1–
523 PM8, respectively; Supplementary Figure S2C, S2D), which are coloured on the PC plots in
524 Fig. 1F-1I. GO term enrichment for RNAs, proteins and PMs in the principal component,
525 clustering and peak time analyses is presented in Supplementary Tables S3-S5, with a

526 summary for proteins and PMs in Supplementary Figure S5. We analysed the distribution of
527 individual peak times (Figure 3) to understand these patterns, starting with the proteins.

528

529 Daytime peaks of protein abundance

530 Hundreds of transcripts reach peak abundance at every timepoint around the day/night cycle
531 (Fig. 3A) (Monnier *et al.*, 2010). In contrast, most protein profiles peaked in the light interval
532 (85% at ZT4-12; Fig. 2B), separating the day and night samples in line with the PC analysis.
533 Metabolic labelling of *O. tauri* has shown ~5-fold higher protein synthesis rates in the day
534 compared to the night (Martin *et al.*, 2012). Consistent with this, our analyses showed
535 translation-related proteins were enriched among the rhythmic proteins with high abundance
536 in the daytime, in PC1, protein cluster P1 and in profiles with daytime peak phase
537 (Supplementary Tables S3-S5, Supplementary Figures S4, S5). We therefore tested whether
538 this light-regulated synthesis alone could explain the observed distribution of protein peaks.

539

540 We simulated protein dynamics (Fig. 2D-2F; Supplementary Figure S6) using measured
541 protein synthesis and degradation rates (Martin *et al.*, 2012), and an even temporal
542 distribution of rhythmic mRNAs. The simulated distribution of protein profiles matched well
543 with our experimental results (Fig. 2E; Supplementary Figures S6D-S6G), with a slightly
544 stronger daytime preference than in the data. *ostta03g04520* is an example of an RNA that
545 peaks at ZT0 and its protein profile (Fig. 2G) was very similar to the predicted protein from
546 such an RNA (Fig. 2D). The overall distribution of protein profiles substantially reflects the
547 light-stimulated translation rate of this organism (see Discussion).

548

549 Unusual, night-time proteins suggest a ‘dark state’

550 An intriguing pattern of protein regulation stood out from the common, daytime abundance.
551 Protein cluster P6 (and P8) included the rare protein profiles that fell at ZT4 (Supplementary
552 Figure S2C), associated with oxidative metabolism and protein transport GO terms
553 (Supplementary Table S4). Four un-annotated, prasinophyte-specific proteins in cluster P6
554 not only peaked at night, but were also among the 11, highest-amplitude profiles of all the
555 rhythmic proteins (Fig. 3A). Their dramatic fall in abundance at ZT4 suggested a
556 destabilisation by light, so we tested whether such proteins would remain stable during
557 several days of dark-adaptation (DA).

558

559 *O. tauri* cells are photo-autotrophic. Their division is entrained by the LD cycle (Farinas *et al.*
560 *et al.*, 2006) and they arrest transcription in prolonged darkness, when they can survive without
561 growth or division (O’Neill *et al.*, 2011). Cell density (optical density at 600nm) in our
562 cultures increased by ~25% after one LD cycle. Cellular protein content was consistent (18-
563 20 pg cell⁻¹) in replicate measures at ZT0 and ZT24 (Fig. 3B). In cultures transferred to three
564 further days of darkness, optical density remained constant but protein content per cell
565 dropped by over 60% on the first day (ZT24 to ZT48) and was then stable to ZT96. This
566 result was suggestive of an altered, but potentially stable, cellular ‘dark state’, which we
567 tested in a further, proteomic timeseries, sampling in darkness at ZT24, 48, 72 and 96.

568

569 The proteomic landscape changed less during dark adaptation (DA) than under a standard LD
570 cycle. 98 of the 865 proteins quantified by LC-MS changed levels more than the average and
571 only 64 (7%) also changed more than 1.5-fold (Supplementary Table S6). The 35
572 significantly-increasing proteins in DA included five transmembrane transporters, a Lon-
573 related protease and two superoxide dismutases, suggestive of nutrient acquisition, protein
574 mobilisation and oxidative stress responses. The four prasinophyte-specific proteins noted

575 above were among the ten most-increasing proteins in DA, confirming their unusual
576 regulation and suggesting a shared function in both standard night-time and the putative ‘dark
577 state’. The most-decreasing among 63 significantly-decreasing proteins in DA was a starch
578 synthase (ostta06g02940). Its abundance declined in the night under LD cycles, as did all 10
579 of the DA-decreasing proteins that were also rhythmic in LD. The largest functional group of
580 depleted proteins comprised 22 cytosolic ribosomal proteins and translation factors
581 (Supplementary Table S6), suggesting that *O. tauri* selectively mobilised this protein pool in
582 darkness.

583

584 The night-abundant, prasinophyte proteins that accumulated in DA, and night-depleted
585 proteins that fell in DA (such as ostta06g02940, above; or PPDK ostta02g04360,
586 Supplementary Figure S7C), suggested that prolonged darkness preserved a night-like state.
587 An alternative explanation was that protein stability in general was altered in the putative
588 dark state. We sought to test that notion, using the protein degradation rates that were
589 previously measured by metabolic labelling in LD conditions (Martin *et al.*, 2012). Falling
590 protein abundance under DA was significantly correlated with higher degradation rates in LD
591 (Fig. 3C; $R = -0.48$, $p=0.004$, $n=34$), even among these abundant, stable proteins. We also
592 tested RNA abundance for a subset of these proteins in DA by qRT-PCR, showing stable
593 levels after one day of prolonged darkness (ZT48; Supplementary Figure S8A). The lack of
594 RNA regulation seemed consistent with the lack of transcription in these conditions (O’Neill
595 *et al.*, 2011). For example, a further prasinophyte-specific protein ostta03g4500 with a stable
596 RNA level and slightly-increasing protein level in DA also had among the lowest protein
597 degradation rates in LD (Fig. 3C), and was among the most-detected proteins in these
598 conditions (Supplementary Figures S2A, S8B). The RNA data and protein degradation rates
599 suggested that the prasinophyte-specific proteins accumulated due to a focussed, regulatory
600 mechanism, rather than generalised refactoring of the proteome (see Discussion).

601

602 A phospho-dawn of protein modification

603 In contrast to the many daytime-peaking protein profiles, 39% of the changing
604 phosphopeptide motifs (PMs) peaked in abundance at ZT0 (Fig. 2C), double the proportion
605 of any other timepoint. The ZT0 samples were harvested before lights-on, so this ‘phospho-
606 dawn’ anticipated the transition and was not due to light-stimulated translation. Other, high-
607 amplitude PM profiles tracked the levels of their cognate proteins, with little evidence of
608 regulated phosphorylation (Fig. 2G). We therefore tested the contribution of protein levels to
609 PM profiles more broadly, among the 138 genes that were quantified in both protein and PM
610 datasets (Supplementary Figures S7A-B). This subset of 261 protein-PM pairings included
611 proteins peaking at all timepoints, and PM profiles that reflected the peak time distribution of
612 the full dataset. 80% of the PMs peaked at different timepoints than their cognate protein
613 (Supplementary Figure S7C; examples in Fig. 2H). The LHC linker protein CP29
614 (ostta01g04940) illustrates one pattern: its protein level rises in the light while a PM is de-
615 phosphorylated (Supplementary Figure S7C) adjacent to a target site of chloroplast kinase
616 STN7 in *Arabidopsis* (Schönberg *et al.*, 2017).

617 To test the phospho-dawn pattern by a different method, we estimated the bulk protein
618 phosphorylation across the diel cycle using protein gel staining (Supplementary Figures S9A-
619 B). The proportion of phosphorylated proteins was lowest in the daytime and increased
620 during the night to peak at ZT0 (Supplementary Figures S9C). Total phosphorylation was
621 therefore broadly consistent with the distribution of PM profiles (Fig. 2C). Taken together,
622 these results indicate that a regulator other than light or protein abundance controls the *O.*

623 *tauri* phosphoproteome before dawn. Below, we report phosphosite sequences that suggested
624 its identity.

625 Functions of proteins with rhythmic phospho-motifs

626 The LD datasets confirmed that protein phosphorylation profiles often diverged from protein
627 abundance. Colour-coding in Fig. 1H shows that clustering of the phospho-motif (PM)
628 profiles aligned with the PC analysis more clearly than for the lower-amplitude, protein
629 profiles (Fig. 1F). The largest cluster PM1 reflected the profiles that peaked in the ZT0
630 timepoint, which PC analysis also highlighted (Supporting Figure S2D). Phosphopeptide
631 enrichment allowed the detection of many regulatory proteins, including PMs on predicted
632 CONSTANS-like B-box transcription factors (OtCOL) related to the plant clock protein
633 TOC1 (Fig. 4), and on the RWP-RK mating-type factor ostta02g04300 (Blanc-Mathieu *et al.*,
634 2017). PM1 also includes the predicted CK2 target site pS10 in the clock protein CCA1
635 (ostta06g02340; Fig. 4), close to the homologous location of a CK2 site in Arabidopsis
636 CCA1 (Lu *et al.*, 2011).

637
638 PMs in cluster PM3 peaked in the light, consistent with many protein profiles (examples in
639 Fig. 2G). PMs on the photoreceptors phototropin and LOV-HK illustrate these daytime
640 profiles (Fig. 4). Protein functions predicted to regulate transcription, metal ion transport and
641 protein phosphorylation are enriched in this cluster (summarised in Supplementary Figure
642 S2F; Supplementary Table S4) and in profiles with daytime peaks (Supplementary Figure
643 S4B; Supplementary Table S5).

644
645 In contrast, the PM2, PM4, PM7 and PM8 clusters peaked at ZT16, with or without
646 accumulation in daytime (Supplementary Figure S2D). These clusters are enriched for PMs
647 on protein kinases including cell-cycle-related kinases (Supplementary Figures S2F, S4B;
648 Supplementary Tables S4 and S5). We therefore analysed the phospho-regulators that might
649 control these profiles, including potential contributions to non-transcriptional timing.

650

651 Phase-specific target sites

652 We first analysed motifs of amino acids that were enriched in rhythmic PMs, compared with
653 all quantified phosphopeptides to avoid potential detection bias due to PM abundance. PMs
654 that peaked at ZT16 were strikingly enriched for the proline-directed motif [pS/pT]P (Fig.
655 5B-C). This strongly implicates the CMGC family of protein kinases, including Cyclin-
656 Dependent Kinases (CDKs) and GSK. Consistent with this, the profiles of PMs with
657 predicted GSK target sequences also most often peaked at ZT16 (Supplementary Figure
658 S10A-B). Levels of *GSK3* RNA and a PM on *GSK3* peaked at ZT12 (Fig. 4), though the
659 auto-phosphorylation site pY210 was not rhythmic (Supplementary Fig. S2B; Supplementary
660 Table S2). More specific CDK target motifs [pS/pT]PXX[K/R] were enriched at ZT12,
661 consistent with the known timing of cell division (Farinas *et al.*, 2006; Moulager *et al.*, 2007)
662 and the peak level of the activation phospho-site of CDKB (Fig. 4). During the day (ZT4 and
663 8), enrichment of hydrophobic residues at positions -5 and +4 is suggestive of the SnRK
664 consensus (Vlad *et al.*, 2008), the plant kinase most related to animal AMPK.

665 In contrast, acid([D/E])-directed target motifs were significantly enriched among the many
666 rhythmic PMs that peaked at ZT0 and the proline-directed motifs were depleted (Fig. 5C).
667 Conversely, these acid-directed motifs were depleted on PMs peaking at ZT16 or ZT4,
668 suggesting a strong phase-specificity. Considering the more specific, predicted target sites for
669 the clock-related protein kinases (Supplementary Figures S10A), predicted CK1 targets were
670 most abundant, and most often peaked at ZT0. Predicted CK2 target sequences were even

671 more phase-specific, with at least 5-fold more peaking at ZT0 than at other times. Thus
672 predicted targets of the clock-related kinases CK1 and CK2 both contribute to the phospho-
673 dawn profiles, in antiphase to the evening peaks of proline-directed phospho-sites.

674 Rhythmic regulation of the kinome

675 The protein abundance of the three detected protein kinases and two phosphatases was not
676 rhythmic (Supplementary Table S1). We therefore analysed the 68 rhythmic PMs on protein
677 kinases and five PMs on protein phosphatases, as candidate mediators of rhythmic
678 phosphorylation (Figs. 5A, 5D). The PMs on kinases represent 8% of the total, though protein
679 kinase genes comprise ~1.5% of the genome. Indeed, the most heavily-phosphorylated
680 protein with 14 PMs was the WITH NO LYSINE (WNK) kinase that might target clock
681 proteins in Arabidopsis (Murakami-Kojima *et al.*, 2002) (Supplementary Table S2;
682 Supplementary Figure S10C). The most-changing PM on a predicted protein phosphatase was
683 pT175 in *ostta1lg02830*, related to human Dual-specificity phosphatase DUSP12 (Fig. 5D).

684 Among the clock-related protein kinases, we note the dusk-peaking PM of GSK3 (above).
685 CK2 subunits were not detected in our data and the PM on CK1 was not strongly rhythmic
686 (Fig. 4). 21 other protein kinases bore rhythmic PMs that are predicted targets of these clock-
687 related kinases (Supplementary Figures S10C).

688 Around mitosis at ZT12-16, significantly peaking PMs were detected on cell cycle regulators
689 CDKA, CDKB and WEE1 (Fig. 5D). Kinase PMs peaking at ZT4-8 included Serine-
690 Arginine Protein Kinases (SRPKs), MAPKs, CDKA and a site on Yet Another Kinase
691 (YAK1). PMs that peaked at ZT0, coincident with the phospho-dawn, included RIO2, YAK1
692 and CDPK, all implicated in cell cycle regulation and progression (Garrett *et al.*, 1991;
693 LaRonde-LeBlanc and Wlodawer, 2005). RIO's are among the few kinase families shared
694 with the Archaea (Kennelly, 2014), making them candidate contributors to an ancient, non-
695 transcriptional oscillator (Edgar *et al.*, 2012).

696 Discussion

697 The diel proteome and phosphoproteome

698 Our results contribute to understand the 'reactive' and 'anticipatory' components of protein
699 regulation in the green lineage under diel (LD) cycles (Mehta *et al.*, 2021). A small fraction
700 of the *O. tauri* proteins quantified here were rhythmic (just under 10%), compared to a
701 majority (58%) of the phosphomotifs (PMs). Most protein profiles peaked in daytime,
702 consistent with the 'reactive' effect predicted from the light-regulated translation that was
703 previously measured in this organism (Martin *et al.*, 2012), and with enrichment of
704 translation-related functions among daytime-peaking proteins. This result reinforces the
705 dangers of using RNA profiles as a proxy for biological function. It further supports our
706 prediction that "translational coincidence" should alter the *O. tauri* proteome in different day
707 lengths, as some rhythmic RNAs will coincide with light-stimulated translation only in long
708 days (Seaton *et al.*, 2018).

709
710 In contrast, the largest number of PM profiles peaked in the pre-dawn, ZT0 timepoint. This
711 anticipatory 'phospho-dawn' might be controlled by the circadian clock. Circadian regulation
712 would be expected to persist under constant conditions, which were not tested here. Studies in
713 Arabidopsis under constant light, however, identified a high fraction of rhythmic
714 phosphopeptides that peaked at subjective dawn (Choudhary *et al.*, 2015)(Krahmer *et al.*,
715 2018), suggesting a similar, circadian-regulated phospho-dawn in higher plants. Such

716 phospho-regulation might prepare green cells for daytime functions and/or end night-time
717 activities, before light-stimulated translation facilitates new protein synthesis.

718 Acid-directed target sites were clearly enriched at ZT0, implicating the clock-related kinases
719 CK1 and CK2 in regulating the phospho-dawn in *O. tauri*. Enrichment of proline-directed
720 target sites occurs in antiphase, at ZT12-16, which implicates the 19 CMGC-class kinase
721 proteins (Hindle *et al.*, 2014) including CDKs, MAPKs and GSK3. These phase-specific
722 enrichments were clearer than in the Arabidopsis studies, suggesting that the minimal kinase-
723 target network of *O. tauri* might be easier to resolve in future. Comparison to the rhythmic
724 phosphoproteome in animals is limited, because the most-rhythmic kinase Akt (also known
725 as Protein Kinase B) in mouse liver (Robles *et al.*, 2016) is absent from the green lineage
726 (Hindle *et al.*, 2014).

727 The low overall rhythmicity (<10%) in the partial proteome quantified here is consistent with
728 similar studies in Arabidopsis, which identified 0.1-1.5% rhythmic proteins from 7-9 % of the
729 proteome in LD, using iTRAQ labelling with similar statistical criteria to ours (Baerenfaller
730 *et al.*, 2015; Baerenfaller *et al.*, 2012), or 4-7% rhythmic proteins from 4% of the proteome
731 under constant light using a gel-based approach (Choudhary *et al.*, 2016). Our results provide
732 11% coverage in the minimal *O. tauri* proteome, with a simpler experimental protocol.
733 Broader coverage of this proteome was reported after our preprint was released (Kay *et al.*,
734 2021), in experiments that included a depletion of abundant proteins, among several technical
735 differences. Their higher reported fraction of rhythmic proteins might reflect the detection of
736 low-abundance proteins and/or analysis with no minimum amplitude threshold.

737

738 [The 'dark state' is indirectly associated with lipid synthesis](#)

739 Among the rhythmic proteins reported here, some of the most highly-regulated were four
740 prasinophyte-specific sequences (unnamed proteins ostta02g03680, ostta03g04960,
741 ostta07g00470, ostta09g00670; Figure 3A) along with ostta03g04500 (Supplementary Figure
742 S2A). These proteins accumulated further in prolonged darkness (Figure 3A). We previously
743 showed that *O. tauri* stop transcription and cell division in those conditions. Cultures resume
744 gene expression and growth upon return to LD cycles, suggesting that dark adaptation
745 induces a state of cellular quiescence. The ecological relevance of a quiescent 'dark state' for
746 photo-autotrophic, surface-dwelling *O. tauri* is not immediately obvious. However,
747 *Ostreococcus* relatives can persist under the Polar Night (Joli *et al.*, 2017), and quiescent
748 forms in other phytoplankton (Roy *et al.*, 2014) can be ecologically important in benthic-
749 pelagic coupling (Marcus and Boero, 1998). Cells near the deep chlorophyll maximum
750 (Cardol *et al.*, 2008) could be moved into the dark, benthic zone by turbulence, to return later
751 via upwelling (Collado-Fabbri *et al.*, 2011; Countway and Caron, 2006). Understanding the
752 laboratory 'dark state' might therefore have ecological relevance.

753 Protein content dropped significantly between 12h and 36h of darkness (ZT24 to ZT48) but
754 was then stable. Proteins associated with cytosolic translation were notably depleted
755 (Supplementary Table 6), rather than abundant, chloroplast proteins involved in
756 photosynthesis. Photosynthetic functions might be particularly important to recover from
757 quiescence, similar to the rapid regrowth observed after nutrient starvation (Liefer *et al.*,
758 2018).

759 A preprint coincident with our first report showed that three of these night-expressed,
760 prasinophyte-specific proteins accumulated strongly in *O. tauri* when the growth medium
761 was depleted of nitrogen, under LD cycles (Smallwood *et al.*, 2018a). The most-depleted
762 protein in their conditions was the same starch synthase (ostta06g02940) that fell most in

763 abundance under our prolonged dark treatment. Nitrogen depletion is commonly used to
764 induce lipid synthesis in algae, in the context of third-generation biofuel production
765 (Zienkiewicz *et al.*, 2016). Prolonged darkness and/or hypoxia can also induce lipid
766 accumulation, and hypoxia can occur in dark-adapting algal cultures due to continued
767 respiration (Hemschemeier *et al.*, 2013). Our culture conditions included sorbitol and
768 glycerol in the growth medium (O'Neill *et al.*, 2011), which are required for viability in
769 prolonged darkness. Our 'dark state' proteome might therefore reflect active lipid synthesis
770 from these substrates.

771 *O. tauri* can form both intracellular lipid droplets and extracellular droplets in membrane-
772 bound 'pea-pod' structures (Smallwood *et al.*, 2018b). Lipid droplets in other algae include
773 major proteins that are restricted to limited taxonomic groups (Zienkiewicz *et al.*, 2016).
774 Some of these are predicted to have all-alpha-helical structure, including the Major Lipid
775 Droplet Protein Cre09.g405500 of *Chlamydomonas reinhardtii* or the Lipid Droplet Surface
776 Protein of the diatom *Nannochloropsis oceanica*. Protein structure homology modelling
777 aligned oस्ता02g03680 with a human BAR domain dimer, an all-helical protein domain that
778 can sense and create membrane curvature (Simunovic *et al.*, 2015)(Supplementary Figure
779 S11), suggesting that this *O. tauri* protein might also be involved in lipid droplets. *N.*
780 *oceanica* lipid synthesis and LDSP accumulation is highly rhythmic but day-phased (Poliner
781 *et al.*, 2015). The night-expressed proteins in *O. tauri* indirectly suggest a different regulation
782 of lipid synthesis, that could have biotechnological relevance.

783 [Supplementary Data Summary](#)

784 **Supplementary Figure S1. Identification of outlier phosphopeptide replicate 4E.**

785

786 **Supplementary Figure S2. Most-detected protein and PM profiles.**

787

788 **Supplementary Figure S3. Changing PMs on non-changing proteins.**

789

790 **Supplementary Figure S4. Clustered protein and PM profiles with enriched functions.**

791

792 **Supplementary Figure S5. Phase-specific GO term enrichment.**

793

794 **Supplementary Figure S6. Simulation of light-regulated translation.**

795

796 **Supplementary Figure S7. Loci identified in both LD protein and phosphopeptide motif
797 datasets.**

798

799 **Supplementary Figure S8. Regulation of proteins tested under Dark Adaptation (DA).**

800

801 **Supplementary Figure S9. Protein and phospho-protein abundance in LD cycle.**

802

803 **Supplementary Figure S10. CK1, CK2 and GSK3 kinase targets and phosphorylation sites in
804 rhythmic kinases.**

805

806 **Supplementary Figure S11. Structural homology of rhythmic, prasinophyte-specific protein.**

807

808 ---

809

810 **Supplementary Table S1. Proteins quantified under LD.**

811

812 **Supplementary Table S2. Phosphopeptide Motifs (PMs) quantified under LD.**

813

814 **Supplementary Table S3. GO term enrichment among RNA, proteins and PMs contributing to**
815 **PCA.**

816

817 **Supplementary Table S4. GO term enrichment among RNA, proteins and PMs in clusters.**

818 Individually-significant, rhythmic protein profiles are considered, to provide sufficient numbers for
819 enrichment analysis. Only BH-corrected significant PM profiles with >1.5-fold changes are
820 considered.

821

822 **Supplementary Table S5. GO term enrichment among rhythmic proteins and PMs by**

823 **peak/trough times.** Only BH-corrected significant protein or PM profiles with >1.5-fold changes are
824 considered.

825

826 **Supplementary Table S6. Proteins quantified under DA.**

827

828 **Acknowledgements**

829 We are very grateful to K. Kis, L. Imrie and D. Kelly for expert technical help, to B. Kolody
830 and A. Dodd for helpful discussion, to M. Hirsch-Hoffmann and K. Baerenfaller for support
831 on pep2pro, and to C.R. Smallwood, J.E. Evans and colleagues for clarifying the comparison
832 to their work. The proteomics analyses were carried out by the EdinOmics research facility
833 (RRID: SCR_021838) at the University of Edinburgh. Funded by the Biotechnology and
834 Biological Sciences Research Council (UKRI-BBSRC award BB/J009423/1). For the
835 purpose of open access, the author has applied a Creative Commons Attribution (CC BY)
836 licence to any Author Accepted Manuscript version arising from this submission.

837 **Author Contributions**

838 Z.B.N. and M.M.H. contributed equally to this study. Investigation and formal analysis,
839 Z.B.N., S.F.M. and T.L.B.; formal analysis (bioinformatics), M.M.H.; formal analysis
840 (mathematical modelling), D.D.S.; conceptualisation and methodology, A.J.M., T.I.S.,
841 T.L.B., S.F.M., M.M.H. and Z.B.N.; funding acquisition and supervision, A.J.M., T.I.S. and
842 T.L.B.; writing, Z.B.N., M.M.H., T.L.B. and A.J.M.

843 **Conflicts of Interest**

844 The authors declare no competing financial interests.

845 **Data Availability**

846 The OTTH95 strain is available from the CCAP (www.ccap.ac.uk) and RCC ([roscoff-culture-](http://roscoff-culture-collection.org)
847 [collection.org](http://roscoff-culture-collection.org)) stock centres. Mass spectrometry proteomics data have been deposited in the
848 ProteomeXchange Consortium via the PRIDE partner repository with the dataset identifiers:
849 LD global proteomics, PXD001735; LD phosphoproteomics, PXD001734; DA global
850 proteomics, PXD002909. The LC-MS data were also previously available in pep2pro at
851 www.pep2pro.ethz.ch (Assemblies 'Ostreococcus tauri Light:dark cycle,LD global',
852 'Ostreococcus tauri Light:dark cycle,LD phospho', 'Ostreococcus tauri dark adaptation,DA
853 global'). Processed data lists are provided in the Supplementary Information.

854

855 **REFERENCES**

856

857 **Baerenfaller K, Massonnet C, Hennig L, Russenberger D, Sulpice R, Walsh S, Stitt M, Granier C,**
858 **Gruissem W.** 2015. A long photoperiod relaxes energy management in Arabidopsis leaf six. *Current*
859 *Plant Biology* **2**, 34–45.

860 **Baerenfaller K, Massonnet C, Walsh S, et al.** 2012. Systems-based analysis of Arabidopsis leaf
861 growth reveals adaptation to water deficit. *Molecular Systems Biology* **8**, 606.

862 **Baginsky S, Gruissem W.** 2009. The chloroplast kinase network: new insights from large-scale
863 phosphoproteome profiling. *Molecular Plant* **2**, 1141–53.

864 **Benjamini Y, Hochberg Y.** 1995. Controlling the False Discovery Rate: A Practical and Powerful
865 Approach to Multiple Testing. *Journal of the Royal Statistical Society: Series B (Methodological)* **57**,
866 289–300.

867 **Blanc-Mathieu R, Verhelst B, Derelle E, et al.** 2014. An improved genome of the model marine alga
868 *Ostreococcus tauri* unfolds by assessing Illumina de novo assemblies. *BMC Genomics* **15**, 1103.

869 **Blasing OE, Gibon Y, Gunther M, Hohne M, Morcuende R, Osuna D, Thimm O, Usadel B, Scheible**
870 **WR, Stitt M.** 2005. Sugars and circadian regulation make major contributions to the global regulation
871 of diurnal gene expression in Arabidopsis. *The Plant Cell* **17**, 3257–81.

872 **Boex-Fontvieille E, Davanture M, Jossier M, Zivy M, Hodges M, Tcherkez G.** 2014. Photosynthetic
873 activity influences cellulose biosynthesis and phosphorylation of proteins involved therein in
874 Arabidopsis leaves. *Journal of Experimental Botany* **65**, 4997–5010.

875 **Bouget FY, Lefranc M, Thommen Q, Pfeuty B, Lozano JC, Schatt P, Botebol H, Verge V.** 2014.
876 Transcriptional versus non-transcriptional clocks: a case study in *Ostreococcus*. *Mar Genomics* **14**,
877 17–22.

878 **Breitkreutz A, Choi H, Sharom JR, et al.** 2010. A global protein kinase and phosphatase interaction
879 network in yeast. *Science* **328**, 1043–6.

880 **Champion A, Kreis M, Mockaitis K, Picaud A, Henry Y.** 2004. Arabidopsis kinome: after the casting.
881 *Funct Integr Genomics* **4**, 163–87.

882 **Chou MF, Schwartz D.** 2011. Biological sequence motif discovery using motif-x. *Curr Protoc*
883 *Bioinformatics* **Chapter 13**, Unit 13 15-24.

884 **Choudhary MK, Nomura Y, Shi H, Nakagami H, Somers DE.** 2016. Circadian Profiling of the
885 Arabidopsis Proteome Using 2D-DIGE. *Frontiers in Plant Science* **7**, 1007.

886 **Choudhary MK, Nomura Y, Wang L, Nakagami H, Somers DE.** 2015. Quantitative Circadian
887 Phosphoproteomic Analysis of Arabidopsis Reveals Extensive Clock Control of Key Components in
888 Physiological, Metabolic, and Signaling Pathways*. *Molecular & Cellular Proteomics* **14**, 2243–2260.

- 889 **Christie JM.** 2007. Phototropin blue-light receptors. *Annual Review of Plant Biology* **58**, 21–45.
- 890 **Corellou F, Schwartz C, Motta J-P, Djouani-Tahri EB, Sanchez F, Bouget F-Y.** 2009. Clocks in the
891 Green Lineage: Comparative Functional Analysis of the Circadian Architecture of the Picoeukaryote
892 *Ostreococcus*. *The Plant Cell* **21**, 3436–3449.
- 893 **Courties C, Vaquer A, Troussellier M, Lautier J, Chrétiennot-Dinet MJ, Neveux J, Machado C,**
894 **Claustre H.** 1994. Smallest eukaryotic organism. *Nature* **370**, 255–255.
- 895 **Cox J, Mann M.** 2008. MaxQuant enables high peptide identification rates, individualized p.p.b.-
896 range mass accuracies and proteome-wide protein quantification. *Nat Biotechnol* **26**, 1367–72.
- 897 **Creux N, Harmer S.** 2019. Circadian Rhythms in Plants. *Cold Spring Harbor Perspectives in Biology* **11**,
898 a034611.
- 899 **Derelle E, Ferraz C, Rombauts S, et al.** 2006. Genome analysis of the smallest free-living eukaryote
900 *Ostreococcus tauri* unveils many unique features. *Proceedings of the National Academy of Sciences*
901 *of the U S A* **103**, 11647–52.
- 902 **Djouani-Tahri el B, Christie JM, Sanchez-Ferandin S, Sanchez F, Bouget FY, Corellou F.** 2011*a*. A
903 eukaryotic LOV-histidine kinase with circadian clock function in the picoalga *Ostreococcus*. *Plant*
904 *Journal* **65**, 578–88.
- 905 **Djouani-Tahri el B, Sanchez F, Lozano JC, Bouget FY.** 2011*b*. A phosphate-regulated promoter for
906 fine-tuned and reversible overexpression in *Ostreococcus*: application to circadian clock functional
907 analysis. *PLoS ONE* **6**, e28471.
- 908 **Doherty MK, Hammond DE, Clague MJ, Gaskell SJ, Beynon RJ.** 2009. Turnover of the Human
909 Proteome: Determination of Protein Intracellular Stability by Dynamic SILAC. *Journal of Proteome*
910 *Research* **8**, 104–112.
- 911 **Dunlap JC, Loros JJ.** 2017. Making Time: Conservation of Biological Clocks from Fungi to Animals.
912 *Microbiol Spectr* **5**.
- 913 **Edgar RS, Green EW, Zhao Y, et al.** 2012. Peroxiredoxins are conserved markers of circadian
914 rhythms. *Nature* **485**, 459–64.
- 915 **Farinas B, Mary C, Manes CLD, Bhaud Y, Peaucellier G, Moreau H.** 2006. Natural synchronisation for
916 the study of cell division in the green unicellular alga *Ostreococcus tauri*. *Plant Molecular Biology* **60**,
917 277–292.
- 918 **Feeney KA, Hansen LL, Putker M, Olivares-Yañez C, Day J, Eades LJ, Larrondo LF, Hoyle NP, O’Neill**
919 **JS, van Ooijen G.** 2016. Daily magnesium fluxes regulate cellular timekeeping and energy balance.
920 *Nature* **532**, 375–379.
- 921 **Garrett S, Menold MM, Broach JR.** 1991. The *Saccharomyces cerevisiae* YAK1 gene encodes a
922 protein kinase that is induced by arrest early in the cell cycle. *Molecular and Cellular Biology* **11**,
923 4045–4052.

- 924 **Hemschemeier A, Casero D, Liu B, Benning C, Pellegrini M, Happe T, Merchant SS.** 2013. COPPER
925 RESPONSE REGULATOR1–Dependent and –Independent Responses of the *Chlamydomonas*
926 *reinhardtii* Transcriptome to Dark Anoxia. *The Plant Cell* **25**, 3186–3211.
- 927 **Hindle MM, Le Bihan T, Krahmer J, Martin SF, Noordally ZB, Simpson TI, Millar AJ.** 2016. qpMerge:
928 Merging different peptide isoforms using a motif centric strategy.
- 929 **Hindle MM, Martin SF, Noordally ZB, van Ooijen G, Barrios-Llerena ME, Simpson TI, Le Bihan T,**
930 **Millar AJ.** 2014. The reduced kinome of *Ostreococcus tauri*: core eukaryotic signalling components in
931 a tractable model species. *BMC Genomics* **15**, 640.
- 932 **Hirsch-Hoffmann M, Gruissem W, Baerenfaller K.** 2012. pep2pro: the high-throughput proteomics
933 data processing, analysis, and visualization tool. *Frontiers in Plant Science* **3**, 123.
- 934 **Ishihara H, Obata T, Sulpice R, Fernie AR, Stitt M.** 2015. Quantifying protein synthesis and
935 degradation in *Arabidopsis* by dynamic ¹³CO₂ labeling and analysis of enrichment in individual
936 amino acids in their free pools and in protein. *Plant Physiology* **168**, 74–93.
- 937 **Ito J, Taylor NL, Castleden I, Weckwerth W, Millar AH, Heazlewood JL.** 2009. A survey of the
938 *Arabidopsis thaliana* mitochondrial phosphoproteome. *Proteomics* **9**, 4229–40.
- 939 **Jones P, Binns D, Chang HY, et al.** 2014. InterProScan 5: genome-scale protein function
940 classification. *Bioinformatics* **30**, 1236–1240.
- 941 **Juntawong P, Bailey-Serres J.** 2012. Dynamic Light Regulation of Translation Status in *Arabidopsis*
942 *thaliana*. *Frontiers in Plant Science* **3**, 66.
- 943 **Karr JR, Sanghvi JC, Macklin DN, Gutschow MV, Jacobs JM, Bolival B, Assad-Garcia N, Glass JI,**
944 **Covert MW.** 2012. A whole-cell computational model predicts phenotype from genotype. *Cell* **150**,
945 389–401.
- 946 **Kay H, Grunewald E, Feord HK, Gil S, Peak-Chew SY, Stangherlin A, O’Neill JS, van Ooijen G.** 2021.
947 Deep-coverage spatiotemporal proteome of the picoeukaryote *Ostreococcus tauri* reveals
948 differential effects of environmental and endogenous 24-hour rhythms. *Commun Biol* **4**, 1147.
- 949 **Kennelly PJ.** 2014. Protein Ser/Thr/Tyr phosphorylation in the Archaea. *Journal of Biological*
950 *Chemistry* **289**, 9480–7.
- 951 **Kessner D, Chambers M, Burke R, Agus D, Mallick P.** 2008. ProteoWizard: open source software for
952 rapid proteomics tools development. *Bioinformatics* **24**, 2534–6.
- 953 **Khoury GA, Baliban RC, Floudas CA.** 2011. Proteome-wide post-translational modification statistics:
954 frequency analysis and curation of the swiss-prot database. *Scientific reports* **1**, 90.
- 955 **Kolody BC, McCrow JP, Allen LZ, et al.** 2019. Diel transcriptional response of a California Current
956 plankton microbiome to light, low iron, and enduring viral infection. *ISME J* **13**, 2817–2833.
- 957 **Krahmer J, Hindle M, Perby LK, Mogensen HK, Nielsen TH, Halliday KJ, van Ooijen G, Le Bihan T,**
958 **Millar AJ.** 2022. The Circadian Clock Gene Circuit Controls Protein and Phosphoprotein Rhythms in
959 *Arabidopsis thaliana*. *Mol Cell Proteomics* **21**, 100172.

- 960 **Kusakina J, Dodd AN.** 2012. Phosphorylation in the plant circadian system. *Trends in Plant Science*
961 **17**, 575–83.
- 962 **Laloum D, Robinson-Rechavi M.** 2022. Rhythmicity is linked to expression cost at the protein level
963 but to expression precision at the mRNA level. *PLOS Computational Biology* **18**, e1010399.
- 964 **Langfelder P, Zhang B, Horvath S.** 2008. Defining clusters from a hierarchical cluster tree: the
965 Dynamic Tree Cut package for R. *Bioinformatics* **24**, 719–720.
- 966 **LaRonde-LeBlanc N, Wlodawer A.** 2005. The RIO kinases: An atypical protein kinase family required
967 for ribosome biogenesis and cell cycle progression. *Biochimica et Biophysica Acta (BBA) - Proteins*
968 *and Proteomics* **1754**, 14–24.
- 969 **Le Bihan T, Hindle M, Martin SF, Barrios-Llerena ME, Krahmer J, Kis K, Millar AJ, van Ooijen G.**
970 2015. Label-free quantitative analysis of the casein kinase 2-responsive phosphoproteome of the
971 marine minimal model species *Ostreococcus tauri*. *Proteomics*.
- 972 **Le Bihan T, Martin SF, Chirnside ES, van Ooijen G, Barrios-Llerena ME, O'Neill JS, Shliaha PV, Kerr**
973 **LE, Millar AJ.** 2011. Shotgun proteomic analysis of the unicellular alga *Ostreococcus tauri*. *J*
974 *Proteomics* **74**, 2060–70.
- 975 **Li L, Nelson CJ, Trosch J, Castleden I, Huang S, Millar AH.** 2017. Protein Degradation Rate in
976 *Arabidopsis thaliana* Leaf Growth and Development. *The Plant Cell* **29**, 207–228.
- 977 **Lu SX, Liu H, Knowles SM, Li J, Ma L, Tobin EM, Lin C.** 2011. A role for protein kinase casein kinase2
978 alpha-subunits in the *Arabidopsis* circadian clock. *Plant Physiology* **157**, 1537–45.
- 979 **Manning G, Whyte DB, Martinez R, Hunter T, Sudarsanam S.** 2002. The protein kinase complement
980 of the human genome. *Science* **298**, 1912–34.
- 981 **Martin SF, Munagapati VS, Salvo-Chirnside E, Kerr LE, Le Bihan T.** 2012. Proteome Turnover in the
982 Green Alga *Ostreococcus tauri* by Time Course (15)N Metabolic Labeling Mass Spectrometry. *J*
983 *Proteome Res* **11**, 476–86.
- 984 **Mehra A, Baker CL, Loros JJ, Dunlap JC.** 2009. Post-translational modifications in circadian rhythms.
985 *Trends Biochem Sci* **34**, 483–90.
- 986 **Mehta D, Krahmer J, Uhrig RG.** 2021. Closing the protein gap in plant chronobiology. *The Plant*
987 *Journal*.
- 988 **Michael TP, Mockler TC, Breton G, et al.** 2008. Network discovery pipeline elucidates conserved
989 time-of-day-specific cis-regulatory modules. *PLoS Genet* **4**, e14.
- 990 **Millar AJ.** 2016. The intracellular dynamics of circadian clocks reach for the light of ecology and
991 evolution. *Annual Review of Plant Biology* **67**, 595–618.
- 992 **Missra A, Ernest B, Lohoff T, Jia Q, Satterlee J, Ke K, von Arnim AG.** 2015. The Circadian Clock
993 Modulates Global Daily Cycles of mRNA Ribosome Loading. *The Plant Cell* **27**, 2582–2599.

- 994 **Monnier A, Liverani S, Bouvet R, Jesson B, Smith JQ, Mosser J, Corellou F, Bouget FY.** 2010.
995 Orchestrated transcription of biological processes in the marine picoeukaryote *Ostreococcus*
996 exposed to light/dark cycles. *BMC Genomics* **11**, 192.
- 997 **Moulager M, Monnier A, Jesson B, Bouvet R, Mosser J, Schwartz C, Garnier L, Corellou F, Bouget**
998 **FY.** 2007. Light-dependent regulation of cell division in *Ostreococcus*: evidence for a major
999 transcriptional input. *Plant Physiology* **144**, 1360–9.
- 1000 **Noordally ZB, Millar AJ.** 2015. Clocks in algae. *Biochemistry* **54**, 171–83.
- 1001 **Ocone A, Millar AJ, Sanguinetti G.** 2013. Hybrid regulatory models: a statistically tractable approach
1002 to model regulatory network dynamics. *Bioinformatics* **29**, 910–6.
- 1003 **O’Neill JS, van Ooijen G, Dixon LE, Troein C, Corellou F, Bouget FY, Reddy AB, Millar AJ.** 2011.
1004 Circadian rhythms persist without transcription in a eukaryote. *Nature* **469**, 554–8.
- 1005 **van Ooijen G, Dixon LE, Troein C, Millar AJ.** 2011. Proteasome Function Is Required for Biological
1006 Timing throughout the Twenty-Four Hour Cycle. *Current Biology* **21**, 869–875.
- 1007 **van Ooijen G, Hindle M, Martin SF, Barrios-Llerena M, Sanchez F, Bouget FY, O’Neill JS, Le Bihan T,**
1008 **Millar AJ.** 2013. Functional analysis of Casein Kinase 1 in a minimal circadian system. *PLoS ONE* **8**,
1009 e70021.
- 1010 **van Ooijen G, Knox K, Kis K, Bouget FY, Millar AJ.** 2012. Genomic transformation of the
1011 picoeukaryote *Ostreococcus tauri*. *J Vis Exp*, e4074.
- 1012 **van Ooijen G, Millar AJ.** 2012. Non-transcriptional oscillators in circadian timekeeping. *Trends*
1013 *Biochem Sci* **37**, 484–92.
- 1014 **O’Shea JP, Chou MF, Quader SA, Ryan JK, Church GM, Schwartz D.** 2013. pLogo: a probabilistic
1015 approach to visualizing sequence motifs. *Nature Methods* **10**, 1211–1212.
- 1016 **Paajanen P, Lane de Barros Dantas L, Dodd AN.** 2021. Layers of crosstalk between circadian
1017 regulation and environmental signalling in plants. *Current Biology* **31**, R399–R413.
- 1018 **Pal SK, Liput M, Piques M, et al.** 2013. Diurnal changes of polysome loading track sucrose content in
1019 the rosette of wild-type *Arabidopsis* and the starchless *pgm* mutant. *Plant Physiology* **162**, 1246–65.
- 1020 **Piques M, Schulze WX, Hohne M, Usadel B, Gibon Y, Rohwer J, Stitt M.** 2009. Ribosome and
1021 transcript copy numbers, polysome occupancy and enzyme dynamics in *Arabidopsis*. *Molecular*
1022 *Systems Biology* **5**, 314.
- 1023 **Poliner E, Panchy N, Newton L, Wu G, Lapinsky A, Bullard B, Zienkiewicz A, Benning C, Shiu S-H,**
1024 **Farré EM.** 2015. Transcriptional coordination of physiological responses in *Nannochloropsis oceanica*
1025 CCMP1779 under light/dark cycles. *The Plant Journal* **83**, 1097–1113.
- 1026 **Robbens S, Derelle E, Ferraz C, Wuyts J, Moreau H, Van de Peer Y.** 2007. The complete chloroplast
1027 and mitochondrial DNA sequence of *Ostreococcus tauri*: organelle genomes of the smallest
1028 eukaryote are examples of compaction. *Mol Biol Evol* **24**, 956–68.

- 1029 **Schönberg A, Rödiger A, Mehwald W, Galonska J, Christ G, Helm S, Thieme D, Majovsky P,**
1030 **Hoehenwarter W, Baginsky S.** 2017. Identification of STN7/STN8 kinase targets reveals connections
1031 between electron transport, metabolism and gene expression. *The Plant Journal* **90**, 1176–1186.
- 1032 **Schuirmann DL.** 1981. On Hypothesis-Testing to Determine If the Mean of a Normal-Distribution Is
1033 Contained in a Known Interval. *Biometrics* **37**, 617–617.
- 1034 **Scott M, Gunderson CW, Mateescu EM, Zhang Z, Hwa T.** 2010. Interdependence of cell growth and
1035 gene expression: origins and consequences. *Science* **330**, 1099–102.
- 1036 **Seaton DD, Graf A, Baerenfaller K, Stitt M, Millar AJ, Gruissem W.** 2018. Photoperiodic control of
1037 the Arabidopsis proteome reveals a translational coincidence mechanism. *Molecular Systems*
1038 *Biology* **14**, e7962.
- 1039 **Smallwood CR, Chen J-H, Kumar N, et al.** 2018a. Integrated systems biology and imaging of the
1040 smallest free-living eukaryote *Ostreococcus tauri*. bioRxiv.
- 1041 **Smallwood CR, Chrisler W, Chen J-H, Patello E, Thomas M, Boudreau R, Ekman A, Wang H,**
1042 **McDermott G, Evans JE.** 2018b. *Ostreococcus tauri* is a high-lipid content green algae that extrudes
1043 clustered lipid droplets. bioRxiv.
- 1044 **Smith SM, Fulton DC, Chia T, Thorneycroft D, Chapple A, Dunstan H, Hylton C, Zeeman SC, Smith**
1045 **AM.** 2004. Diurnal changes in the transcriptome encoding enzymes of starch metabolism provide
1046 evidence for both transcriptional and posttranscriptional regulation of starch metabolism in
1047 Arabidopsis leaves. *Plant Physiology* **136**, 2687–99.
- 1048 **Troein C, Corellou F, Dixon LE, van Ooijen G, O'Neill JS, Bouget F-Y, Millar AJ.** 2011. Multiple light
1049 inputs to a simple clock circuit allow complex biological rhythms. *The Plant Journal* **66**, 375–385.
- 1050 **Turkina MV, Kargul J, Blanco-Rivero A, Villarejo A, Barber J, Vener AV.** 2006. Environmentally
1051 modulated phosphoproteome of photosynthetic membranes in the green alga *Chlamydomonas*
1052 *reinhardtii*. *Mol Cell Proteomics* **5**, 1412–25.
- 1053 **Uhrig RG, Echevarría-Zomeño S, Schlapfer P, Grossmann J, Roschitzki B, Koerber N, Fiorani F,**
1054 **Gruissem W.** 2021. Diurnal dynamics of the Arabidopsis rosette proteome and phosphoproteome.
1055 *Plant, Cell & Environment* **44**, 821–841.
- 1056 **Vizcaino JA, Csordas A, del-Toro N, et al.** 2016. 2016 update of the PRIDE database and its related
1057 tools. *Nucleic Acids Research* **44**, D447-56.
- 1058 **Vizcaino JA, Deutsch EW, Wang R, et al.** 2014. ProteomeXchange provides globally coordinated
1059 proteomics data submission and dissemination. *Nature Biotechnology* **32**, 223–6.
- 1060 **Vlad F, Turk BE, Peynot P, Leung J, Merlot S.** 2008. A versatile strategy to define the
1061 phosphorylation preferences of plant protein kinases and screen for putative substrates. *The Plant*
1062 *Journal* **55**, 104–117.
- 1063 **Ward JH.** 1963. Hierarchical Grouping to Optimize an Objective Function. *Journal of the American*
1064 *Statistical Association* **58**, 236-.

- 1065 **Westlake WJ.** 1981. Bioequivalence Testing - a Need to Rethink - Reply. *Biometrics* **37**, 591–593.
- 1066 **Whitelam GC, Halliday KJ.** 2007. *Light and plant development*. Oxford ; Ames, Iowa: Blackwell Pub.
- 1067 **Wong DC, O’Neill JS.** 2018. Non-transcriptional processes in circadian rhythm generation. *Curr Opin*
1068 *Physiol* **5**, 117–132.
- 1069 **Xue Y, Liu Z, Cao J, Ma Q, Gao X, Wang Q, Jin C, Zhou Y, Wen L, Ren J.** 2011. GPS 2.1: enhanced
1070 prediction of kinase-specific phosphorylation sites with an algorithm of motif length selection.
1071 *Protein Eng Des Sel* **24**, 255–60.
- 1072 **Yang J, Zhang Y.** 2015. Protein Structure and Function Prediction Using I-TASSER. *Curr Protoc*
1073 *Bioinformatics* **52**, 5 8 1-15.
- 1074 **Zienkiewicz K, Du Z-Y, Ma W, Vollheyde K, Benning C.** 2016. Stress-induced neutral lipid
1075 biosynthesis in microalgae — Molecular, cellular and physiological insights. *Biochimica et Biophysica*
1076 *Acta (BBA) - Molecular and Cell Biology of Lipids* **1861**, 1269–1281.
- 1077

1078 FIGURE LEGENDS

1079 **Figure 1. Daily variation in transcripts, proteins, and phosphopeptide motifs.** (A) Workflow for
1080 proteomics in *O. tauri* under LD. Overlap in (B) detected and quantified gene loci, (C) significantly
1081 changing (solid circles) or not significantly-changing (dashed circles) loci for transcripts (Monnier *et*
1082 *al.*, 2010), proteins and PMs; genomic loci excluded (square brackets). (D-I) Bi-plots of PCA for (D,
1083 E) transcript, (F, G) protein and (H, I) phosphomotif profiles. Proportion of the variance for each PC
1084 is indicated. Dot locations show the weighting of each RNA/protein/PM in each PC; colours show the
1085 assigned cluster (as in Supplementary Figure S4).

1086
1087 **Figure 2. Distribution of rhythmic protein and phosphopeptide motif peaks, with examples.**
1088 Temporal distribution of peaking profiles in (A) transcripts, (B) proteins and (C) PMs. (D, F)
1089 Simulated protein profiles from RNAs peaking at (D) ZT0 or (F) ZT16, with (red line) or without
1090 light-regulated translation (black line). (E) predicted distribution of protein peak times, with light-
1091 regulated translation. Examples of genes with (G) high-amplitude and similar protein (solid line) and
1092 PM profiles (coloured lines), or (H) PM profiles that differ from the protein profile. (G, H) protein
1093 and PM, left axis; RNA profile (dashed line), right axis. Error bars, S.E. Light/dark indicated by
1094 white/black bars.

1095
1096 **Figure 3. Regulation of dark-accumulating proteins.** Protein abundance profiles (A) of rhythmic
1097 prasinophyte-specific proteins in cluster P6 in LD and DA conditions. (B) Optical density (OD600;
1098 line, right axis) and total protein per cell (columns, left axis) under LD and DA conditions. (C)
1099 Correlation of protein degradation rates (Martin *et al.*, 2012) and relative protein levels after DA;
1100 chloroplast proteins (circles, chloroplast-encoded have solid outline); mitochondrial proteins
1101 (triangles, mitochondria-encoded outlined); PLP-enzymes (squares, marked in legend); prasinophyte-
1102 specific proteins (diamonds).

1103
1104 **Figure 4. Protein and phosphopeptide motif regulation.**
1105 Phosphomotif (coloured lines) and RNA profiles (Monnier *et al.*, 2010)(dashed lines) of the
1106 photoreceptors, clock components, transcription factors and kinases indicated, under LD. Left axis
1107 range 2^6 (64-fold) except OtCCA1 (PM changes 150-fold) and OtCOL2 (PMs change up to 20-fold).
1108 Right (RNA) axis range 12, for log2 data ($2^{12}=4096$ -fold in untransformed data). Error bars, S.E.
1109 Light/dark indicated by white/black bars. PHOT, phototropin photoreceptor; LOV-HK, LOV domain
1110 – histidine kinase photoreceptor; COL, CONSTANS-like transcription factor.

1111
1112 **Figure 5. Motif enrichment and rhythmic protein kinases and phosphatases under LD.** (A)
1113 Rhythmic PMs peaking at each timepoint on protein kinase (black) and phosphatase (grey) proteins
1114 (numbers). (B) Enrichment of proline-directed motifs, for kinases shown in the legend (dashed line, *p*-
1115 value = 0.05). (C) pLogo sequence motifs of rhythmic PMs peaking at each timepoint (foreground;
1116 fg), relative to all detected phosphopeptides (background; bg). ± 3.80 indicates *p*-value = 0.05,
1117 residues above and below axis are over- and under-represented, respectively. (D) Rhythmic PMs by
1118 kinase/phosphatase family, annotated with example proteins.

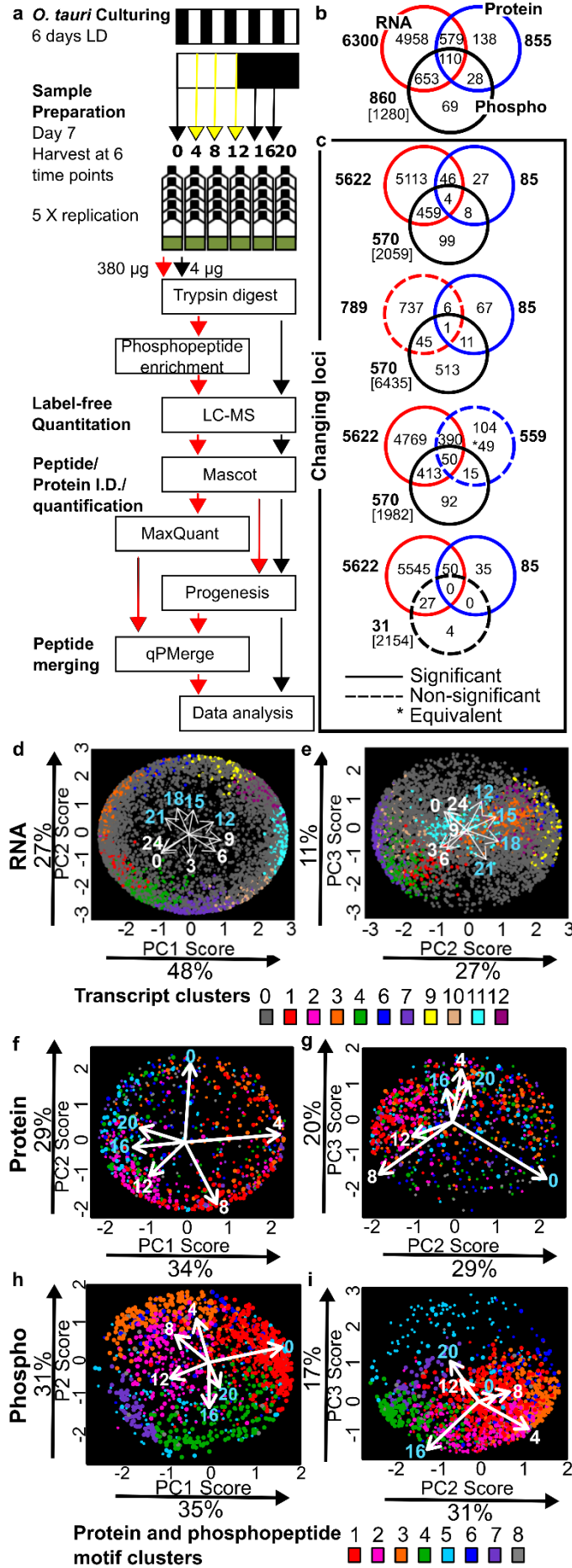
1119

1120

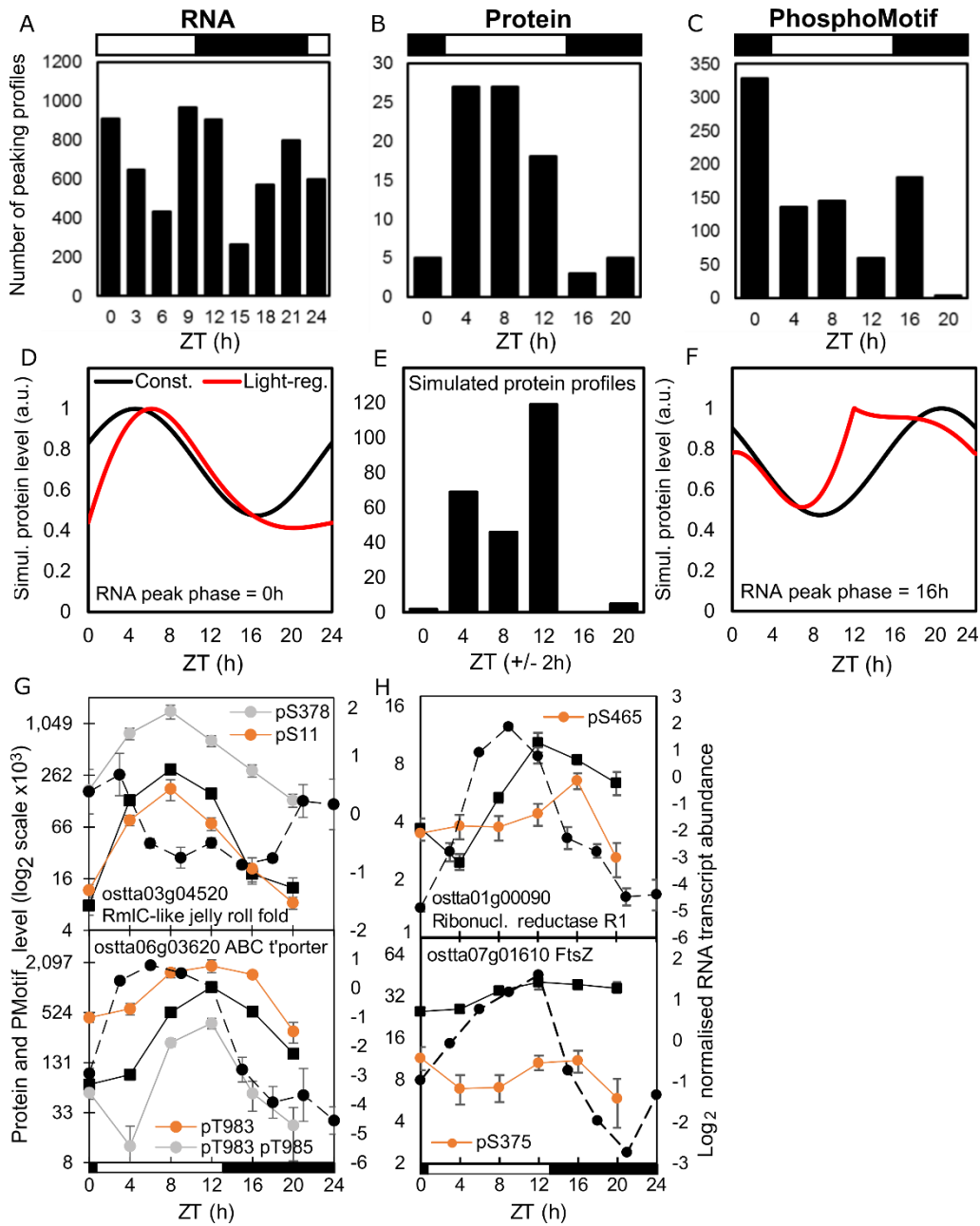
1121 FIGURES

1122 Figure 1

1123



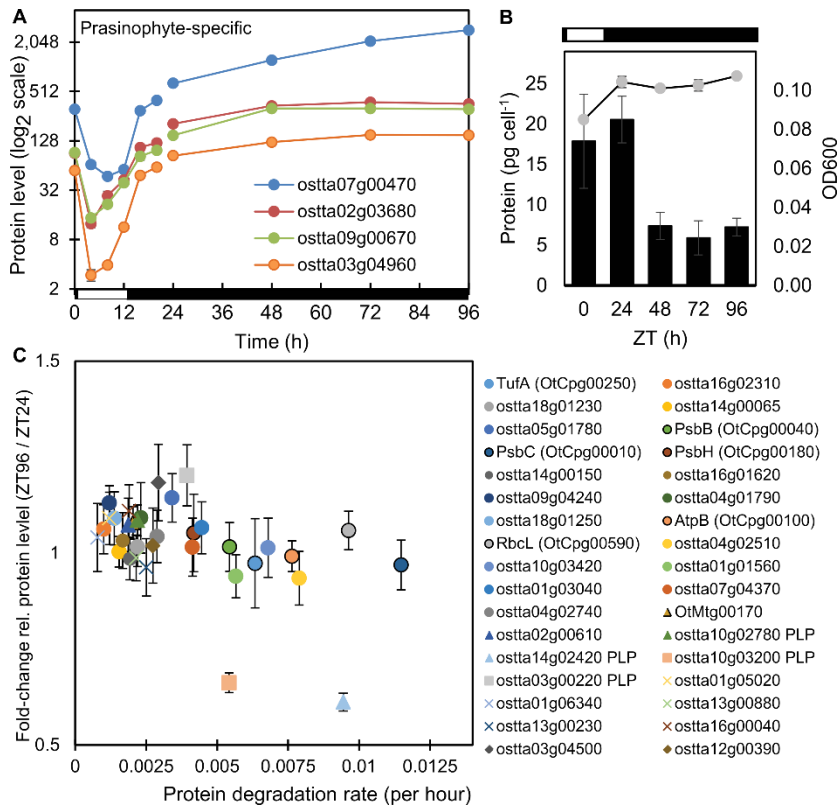
1124 **Figure 2**
 1125
 1126



1127
 1128
 1129

1130
1131
1132

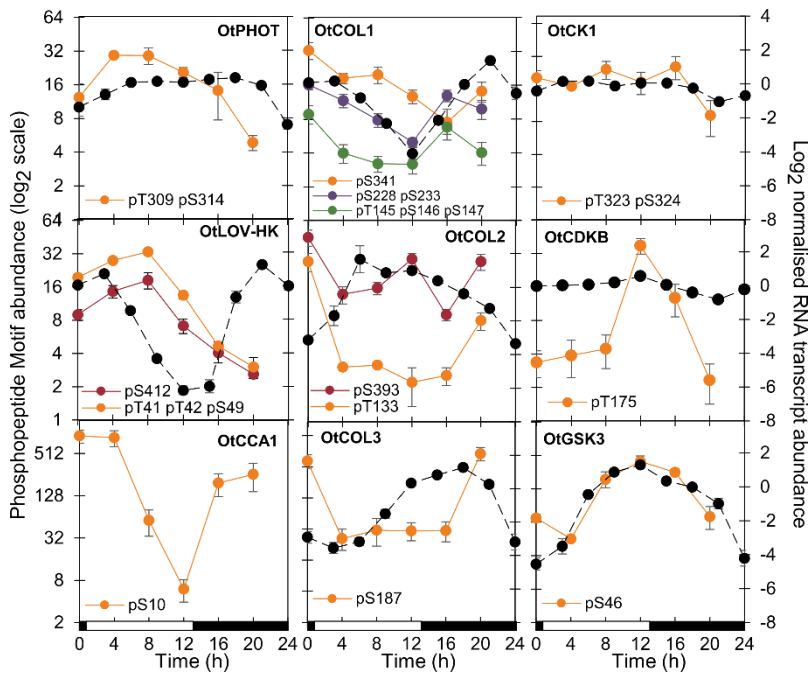
Figure 3



1133
1134

1135 **Figure 4**

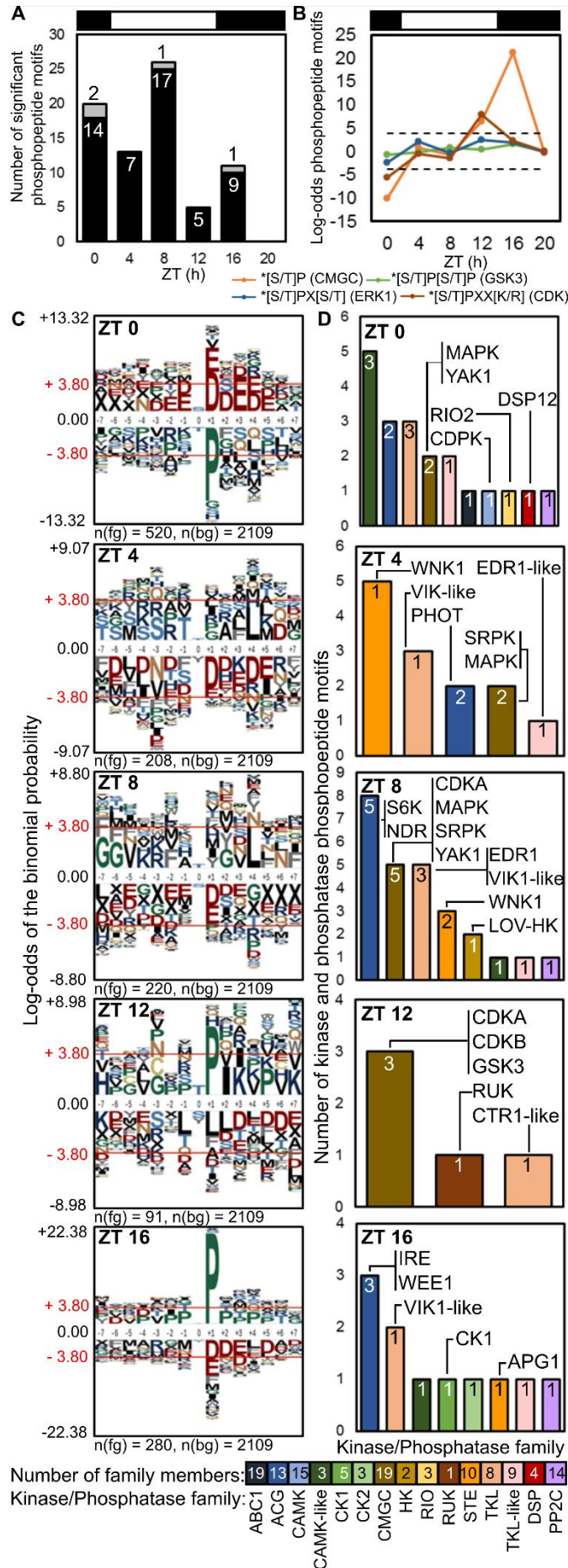
1136



1137

1138

1139 **Figure 5**
1140



1141 Supplementary Figure Legends

1142

1143 **Supplementary Figure S1. Identification of outlier phosphopeptide replicate 4E.** Pearson's
1144 correlation for (a) proteins and (b) phosphopeptide motifs and sample replicate r^2 respective to median
1145 abundance at a ZT for (c) proteins and (d) phosphopeptide motifs. Note differing scales in (a,b), (c,d).

1146

1147 **Supplementary Figure S2. Most-detected protein and PM profiles, with comprehensive heat
1148 maps, clusters and enriched functions.** Highly-abundant proteins (a) and PMs (b) under LD
1149 conditions (* marks rhythmic PMs). Error bars, S.E. Light/dark indicated by white/black bars, above.

1150

1151 **Supplementary Figure S3. Changing PMs on non-changing proteins.** Significantly non-changing
1152 proteins (black lines) determined by two one-sided tests (TOST; $\epsilon = 0.3$), plotted with their rhythmic
1153 phosphopeptide motifs \pm S.E., square brackets show phosphorylated residue. Light/dark indicated by
1154 white/black bars.

1155

1156 **Supplementary Figure S4. Clustered protein and PM profiles with enriched functions.** Heat
1157 maps of median-normalised (A) protein and (B) PM abundance, with insets top left showing the
1158 distribution of levels and colour scale. Clusters P1-8 or PM1-8 are shown, colours in 'cluster' track
1159 are as in Fig. 1; FDR track shows >1.5 fold-change and BH FDR adjusted p -value <0.05 (black line)
1160 or <0.01 (orange line); bars to right of each panel show the mean protein or PM abundance (\log_{10}
1161 scale). Light/dark indicated by white/black bars, above. (C, D) Examples of significantly-changing
1162 proteins and PMs in each cluster (as noted in the main text).

1163

1164 **Supplementary Figure S5. GO enrichments for peaks and troughs.** GO Biological Process term
1165 enrichment for rhythmic (a) proteins and (b) phosphopeptide motifs, that was significant (Fisher's
1166 exact test p -value <0.05) in profiles with peak (no shading) or trough (pink shading) time at each
1167 timepoint. Light/dark indicated by white/black column. Grey bars represent proportion of significant
1168 terms identified with respect to total number of background annotated terms.

1169

1170 **Supplementary Figure S6. Simulation of light-regulated translation.** (a-c) Simulation of protein
1171 dynamics for an RNA with peak expression at ZT0 (a), ZT8 (b) and ZT16 (c), with observed, light-
1172 regulated translation rate (red lines) or with constant translation rate (black lines). Distribution of
1173 protein peaks (d,f) and troughs (e,g) for the model with light-regulated translation (d,e) compared to
1174 data (f,g). Distributions for constant translation would reflect the distribution of RNA profiles.

1175

1176 **Supplementary Figure S7. Loci identified in both LD protein and phosphopeptide motif
1177 datasets.** (a, b) Peak time is compared for genes identified in both LD protein and phosphopeptide
1178 motif datasets, with examples (c). (a) Mixed phase: multiple PMs, peaking at same and different times
1179 from cognate protein. Green shading in (b) follows number per bin. Plotting conventions in (c) follow
1180 Fig. 2c, 2d.

1181

1182 **Supplementary Figure S8. Regulation of proteins tested under Dark Adaptation (DA).**
1183 For ten proteins compared in the DA and metabolic labelling (Martin *et al.*, 2012) data (Fig. 4c), (a)
1184 RNA abundance under LD and DA conditions from qRT-PCR assays, and (b) protein profiles under
1185 LD. *, rhythmic proteins. Error bar, S.E.

1186

1187 **Supplementary Figure S9. Protein and phospho-protein abundance in LD cycle.** Stained gels
1188 showing changes in (a) protein and (b) phosphorylated protein abundance in LD, with (c) ratio of
1189 quantified, phosphorylated protein to total protein intensity.

1190

1191 **Supplementary Figure S10. CK1, CK2 and GSK3 kinase targets and phosphorylation sites in
1192 rhythmic kinases.** Distribution of GPS3-predicted CK1 (black), CK2 (red) and GSK3 (black) targets
1193 among rhythmic phosphopeptide motifs, binned by peak (a) and trough (b) times. (c) Phosphosites on
1194 rhythmic protein kinases predicted to be phosphorylated by CK1, CK2 and GSK3, site location labels

1195 coloured as in (a). * sites first reported here; †‡ sites observed previously (van Ooijen *et al.*, 2013).
1196 Protein kinase classes are coloured as in Figure 5.

1197

1198 **Supplementary Figure S11. Structural homology of a rhythmic prasinophyte-specific protein.**

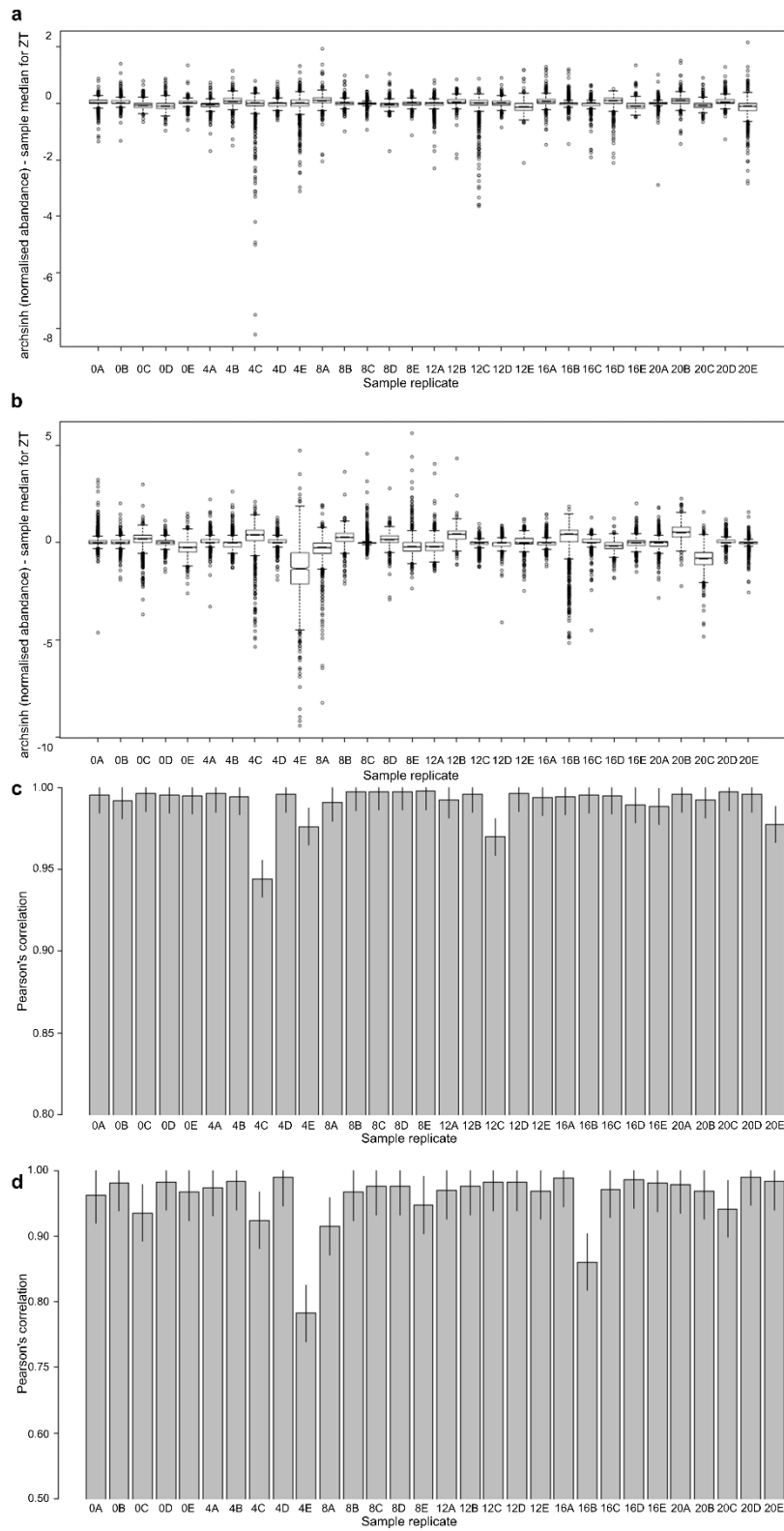
1199 Structural homology models predicted using I-TASSER of (a) ostta02g03680 where the model is
1200 overlaid with (b) *H. sapiens* BAR domain structure (2d4c). Model α -helices (purple) and β -sheets
1201 (green) are numbered in black on the *O. tauri* model and in blue where structure is conserved with
1202 homologue protein overlay and in white where secondary structure is not conserved.

1203

1204 **Supplementary Figures**

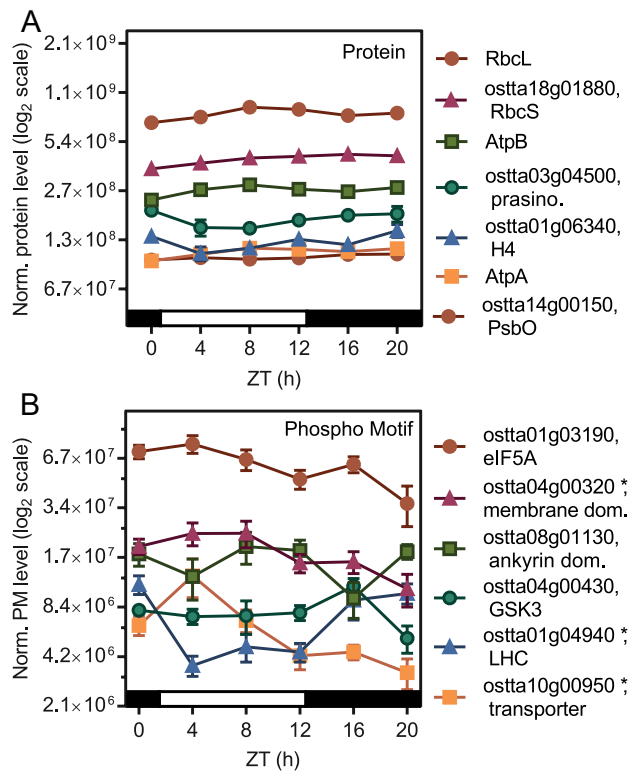
1205 **Supplementary Figure S1**

1206

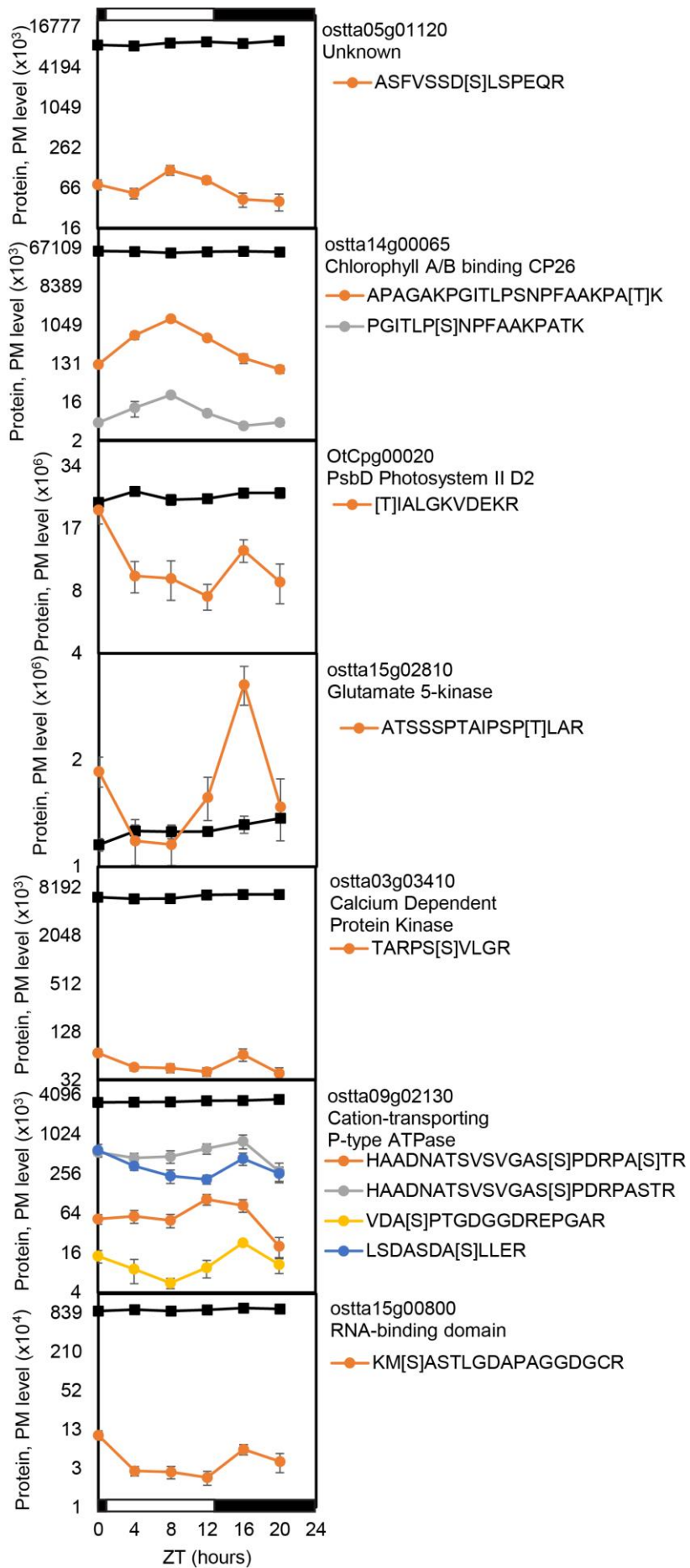


1207 **Supplementary Figure S2**

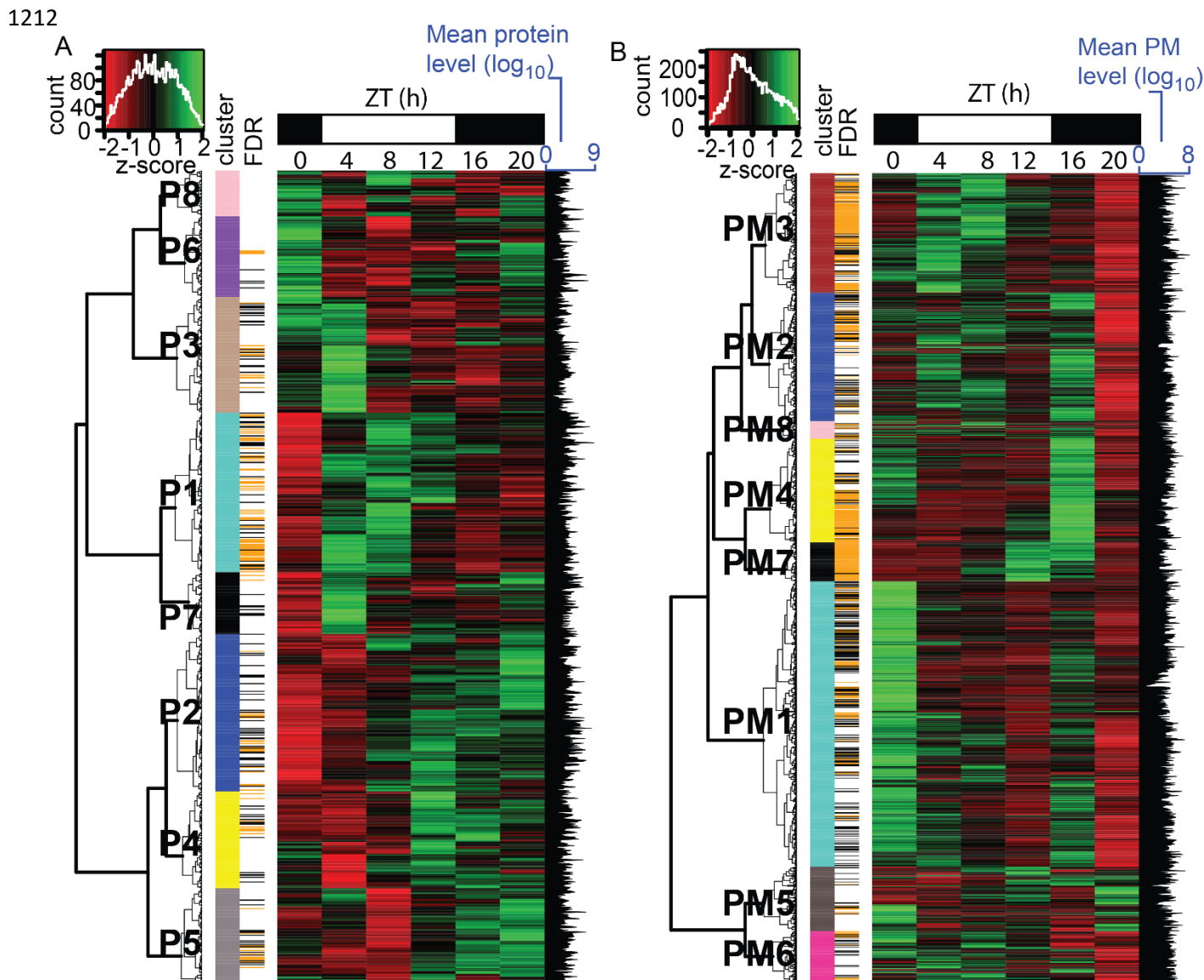
1208



1209 **Supplementary Figure S3**
1210



1211 **Supplementary Figure S4**



C PROTEIN CLUSTERS

P1 Ribosomal subunits, translation initiation/elongation
P2 Thioredoxin-like, FNR, PGK, GAPDH, RuBisCO, PPK, malate dehydrogenase CBM20, PLP transferase
P3 Chlorophyll A/B binding, PSII PsbM
P4 PLP transferases, SSII
P5 Thioredoxin-like, SQR/FR cytochrome b5, phosphogluconate dehydrogenase, transaldolase, aldehyde dehydrogenase
P6 Prasinophyte specific, NH_4^+ transporter
P7 Cytochrome b6, ribosomal subunits, translation initiation/elongation

D PHOSHOPEPTIDE MOTIF CLUSTERS

PM1 TFs, ZF, Myb; cold-shock protein; Zn, Na/solute, Mg^{2+} , transport; AGC, YAK1, CAMK-like, RIO2, CDPK; PIPK; PsaM
PM2 TFs, ZF; eIFs; MAPK, APG1, NDR, AGC, CAMK-like; PP2C; 6-phosphofructo-2-kinase; Ca ATPase
PM3 TFs, ZFs; eIFs; chlorophyll A/B binding, RubisCO activase; thioredoxin; K, Mg, ABC transport; FHA; AGC, SRPK, CDKA, CDKC; PIPK
PM4 TFs ZF; PEP carboxylase proteasome; NO_3^- , Mg transport; WEE1, IRE, MAPK; PIPK
PM5 TFs, CO; GAPDH; chlorophyll A/B binding; Asn synthetase; T6P synthase;
PM6 eIFs, ribosome biogenesis; S6K; PIPK, dacylglycerol kinase
PM7 CDKA, CDKB, GSK3; PPK; phospholipid ATPase
PM8 WNK1, EDR1, CDK regulatory subunit

1213 **Supplementary Figure**
 1214 **S5**
 1215

a Protein - Biological Process

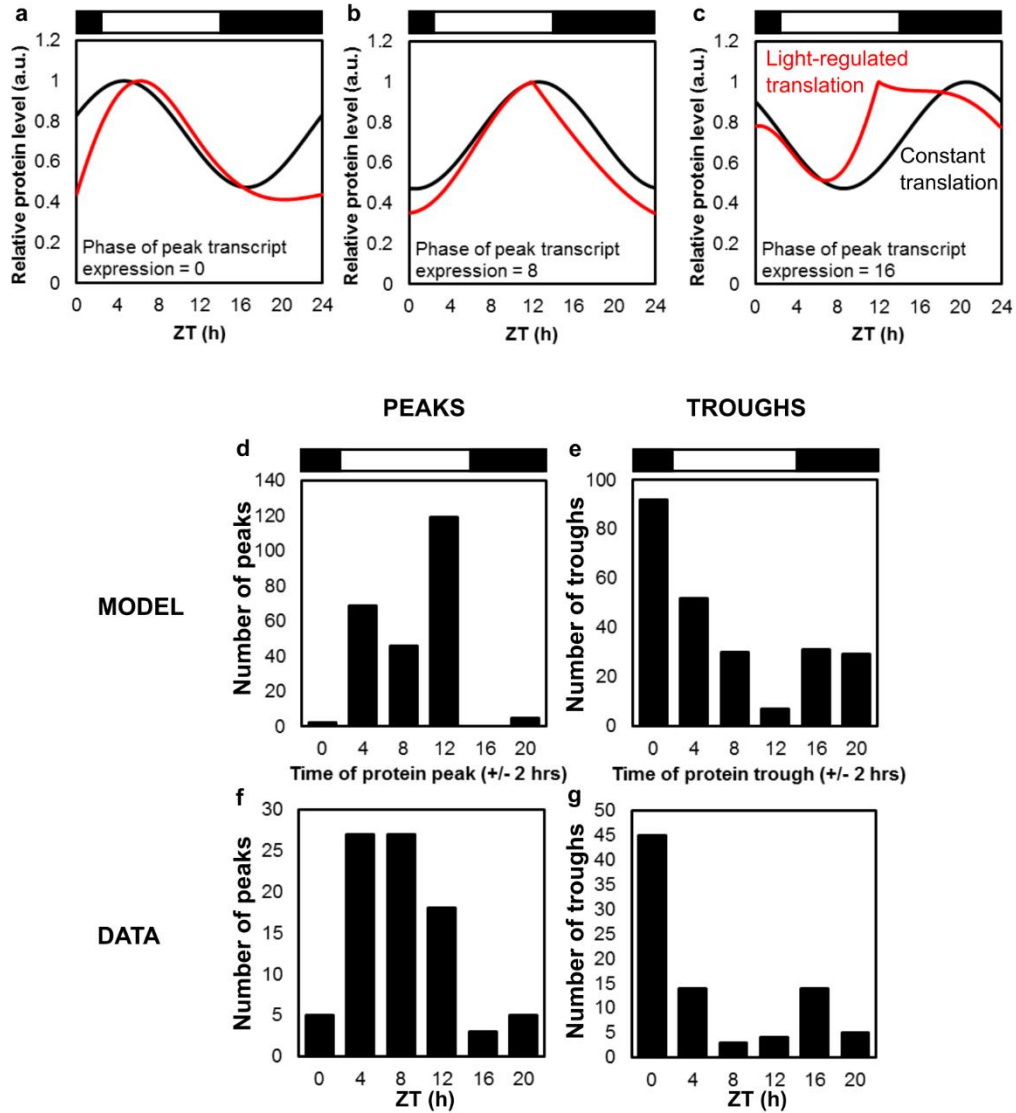
ZT	GO.ID	Term	Annotated	Significant	Expected	p-value
0	GO:0098662	inorganic cation transmembrane transport	17	1	0.1	9.40E-02
	GO:0006412	translation	116	17	6.8	1.30E-04
4	GO:0006412	translation	116	16	4.82	1.30E-06
	GO:0006414	translational elongation	8	2	0.33	4.00E-02
	GO:0006260	DNA replication	3	3	0.04	1.40E-06
8	GO:0015995	chlorophyll biosynthetic process	7	4	0.24	3.10E-05
	GO:0006414	translational elongation	8	2	0.27	2.70E-02
	GO:0006412	translation	116	9	3.95	3.00E-02
	GO:0006418	tRNA aminoacylation for protein translation	15	1	0.03	2.80E-02
12	GO:0006260	DNA replication	3	3	0.07	1.20E-05
	GO:1901606	alpha-amino acid catabolic process	5	2	0.12	4.50E-02
	GO:0090150	establishment of protein localization to membrane	4	1	0.02	2.30E-02
20	GO:0015995	chlorophyll biosynthetic process	7	1	0.04	3.90E-02
	GO:0006414	translational elongation	8	1	0.05	4.50E-02

b Phosphopeptide motifs - Biological Process

ZT	GO.ID	Term	Annotated	Significant	Expected	p-value	
0	GO:0035556	intracellular signal transduction	17	6	3.38	3.10E-03	
	GO:0046488	phosphatidylinositol metabolic process	6	4	1.19	8.10E-03	
	GO:0006457	protein folding	4	3	0.79	1.55E-02	
	GO:0006413	translational initiation	4	3	0.79	1.55E-02	
	GO:0006468	protein phosphorylation	48	14	9.53	1.62E-02	
	GO:0050896	response to stimulus	34	11	6.75	2.49E-02	
	GO:0034622	cellular macromolecular complex assembly	5	3	0.99	2.69E-02	
	GO:0055085	transmembrane transport	38	12	7.55	3.23E-02	
	GO:0015031	protein transport	22	7	4.37	3.29E-02	
	GO:0006352	DNA-templated transcription, initiation	5	3	0.99	3.42E-02	
	GO:0006468	protein phosphorylation	48	5	1.17	2.60E-03	
	4	GO:0055085	transmembrane transport	38	11	3.97	1.20E-05
		GO:0006355	regulation of transcription, DNA-templated	22	8	2.3	7.50E-05
		GO:0000160	phosphorelay signal transduction system	6	3	0.63	6.70E-03
GO:0008152		metabolic process	231	29	24.15	1.20E-02	
GO:0072525		pyridine-containing compound biosynthetic process	3	2	0.31	1.57E-02	
GO:0044271		cellular nitrogen compound biosynthetic process	46	12	4.81	2.07E-02	
GO:0009108		coenzyme biosynthetic process	5	2	0.52	4.74E-02	
GO:0006355		regulation of transcription, DNA-templated	22	6	1.3	6.10E-04	
GO:0009168		purine ribonucleoside monophosphate biosynthetic process	3	2	0.18	8.20E-03	
GO:0009152		purine ribonucleotide biosynthetic process	4	2	0.24	1.58E-02	
GO:0046129		purine ribonucleoside biosynthetic process	4	2	0.24	1.58E-02	
GO:0034654		nucleobase-containing compound biosynthetic process	40	10	2.37	4.11E-02	
GO:0006813		potassium ion transport	7	2	0.41	5.01E-02	
8		GO:0006468	protein phosphorylation	48	18	4.93	8.40E-10
	GO:0032012	regulation of ARF protein signal transduction	3	2	0.31	1.80E-02	
	GO:0005992	trehalose biosynthetic process	3	2	0.31	1.80E-02	
	GO:0006355	regulation of transcription, DNA-templated	22	5	2.26	2.50E-02	
	GO:0006511	ubiquitin-dependent protein catabolic process	3	2	0.13	4.10E-03	
	GO:0007017	microtubule-based process	4	2	0.17	8.00E-03	
	GO:1901362	organic cyclic compound biosynthetic process	46	3	2	2.01E-02	
	GO:0044238	primary metabolic process	192	12	8.36	2.87E-02	
	GO:0098662	inorganic cation transmembrane transport	9	2	0.39	4.29E-02	
	12	GO:0006261	DNA-dependent DNA replication	3	2	0.11	3.10E-03
GO:0006468		protein phosphorylation	48	5	1.84	1.58E-02	
GO:0006396		RNA processing	7	2	0.27	1.98E-02	
GO:0006974		cellular response to DNA damage stimulus	10	2	0.38	3.19E-02	
GO:0019219		regulation of nucleobase-containing compound metabolic process	23	2	0.88	3.26E-02	
GO:0006457		protein folding	4	3	0.28	8.70E-04	
16	GO:0050896	response to stimulus	34	6	2.37	2.99E-02	
	GO:0008152	metabolic process	231	27	16.1	4.15E-02	
	GO:0006281	DNA repair	9	5	1.08	8.20E-04	
	GO:0006310	DNA recombination	4	3	0.48	3.65E-03	
	GO:0009168	purine ribonucleoside monophosphate biosynthetic process	3	2	0.36	2.82E-02	
	GO:0006468	protein phosphorylation	48	9	5.77	4.15E-02	
20	GO:0006355	regulation of transcription, DNA-templated	22	3	0.5	8.60E-03	
	GO:0007165	signal transduction	19	2	0.43	3.91E-02	
	GO:0006412	translation	11	1	0.02	1.90E-02	
	GO:0006468	protein phosphorylation	48	28	16.64	2.80E-07	
	GO:0055085	transmembrane transport	38	20	13.17	7.50E-05	
	GO:0006355	regulation of transcription, DNA-templated	22	13	7.63	5.60E-04	
	GO:0008152	metabolic process	231	105	80.09	8.70E-04	
	GO:0016310	phosphorylation	52	32	18.03	2.27E-03	
	GO:0000160	phosphorelay signal transduction system	6	5	2.08	4.50E-03	
	GO:0046488	phosphatidylinositol metabolic process	6	5	2.08	4.50E-03	
	GO:0009058	biosynthetic process	83	45	28.78	8.60E-03	
	GO:0006796	phosphate-containing compound metabolic process	76	42	26.35	9.00E-03	
	GO:0044249	cellular biosynthetic process	76	40	26.35	9.53E-03	
	GO:0035556	intracellular signal transduction	17	13	5.89	1.31E-02	
GO:0006812	cation transport	22	11	7.63	1.45E-02		
GO:0006352	DNA-templated transcription, initiation	5	4	1.73	1.54E-02		
GO:0009108	coenzyme biosynthetic process	5	4	1.73	1.54E-02		
GO:0072525	pyridine-containing compound biosynthetic process	3	3	1.04	1.55E-02		
GO:0032012	regulation of ARF protein signal transduction	3	3	1.04	1.55E-02		
GO:0030258	lipid modification	3	3	1.04	1.55E-02		
GO:0090407	organophosphate biosynthetic process	9	4	3.12	1.57E-02		
GO:0044711	single-organism biosynthetic process	28	14	9.71	4.57E-02		

1216 **Supplementary Figure S6**

1217



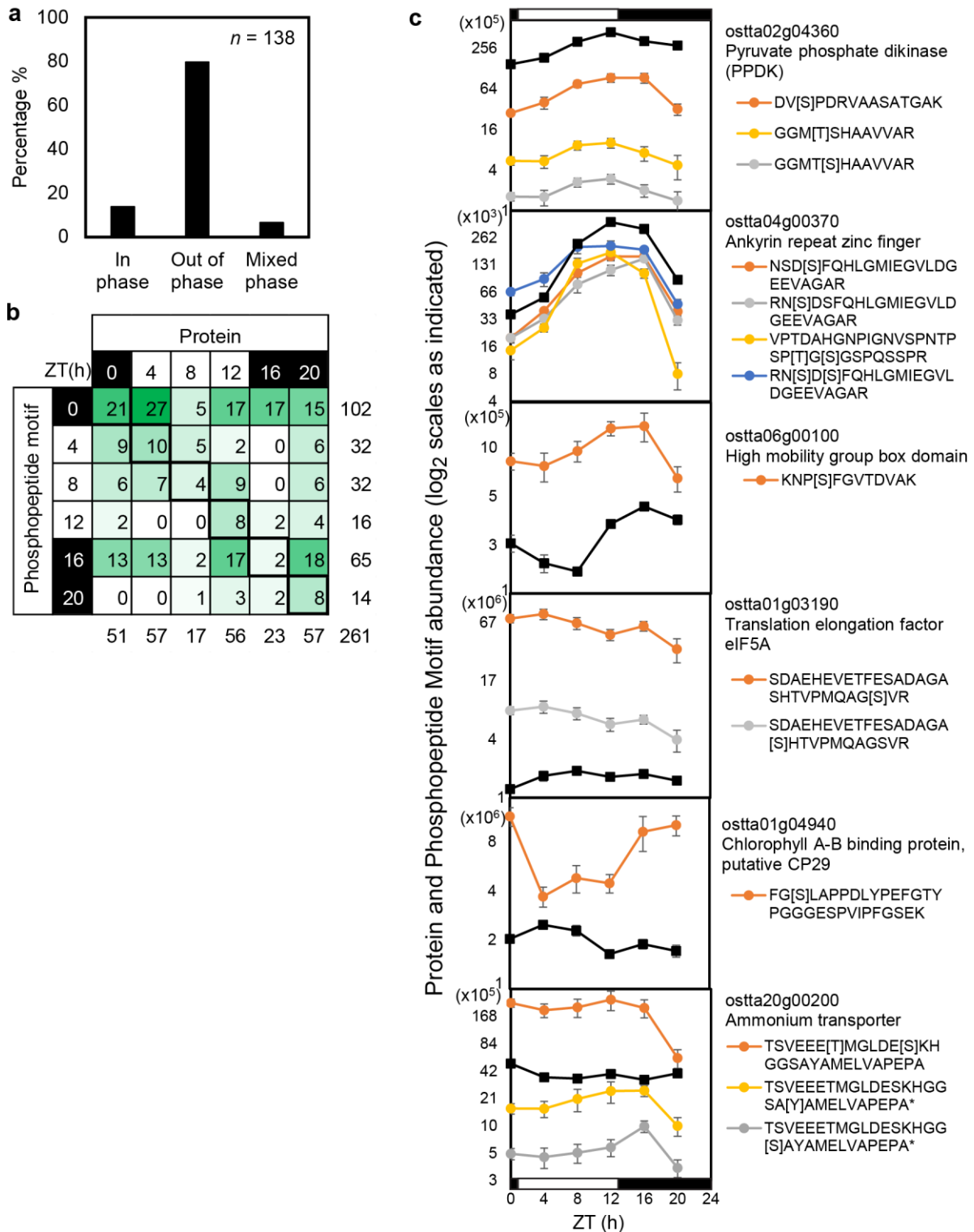
1218

1219

1220

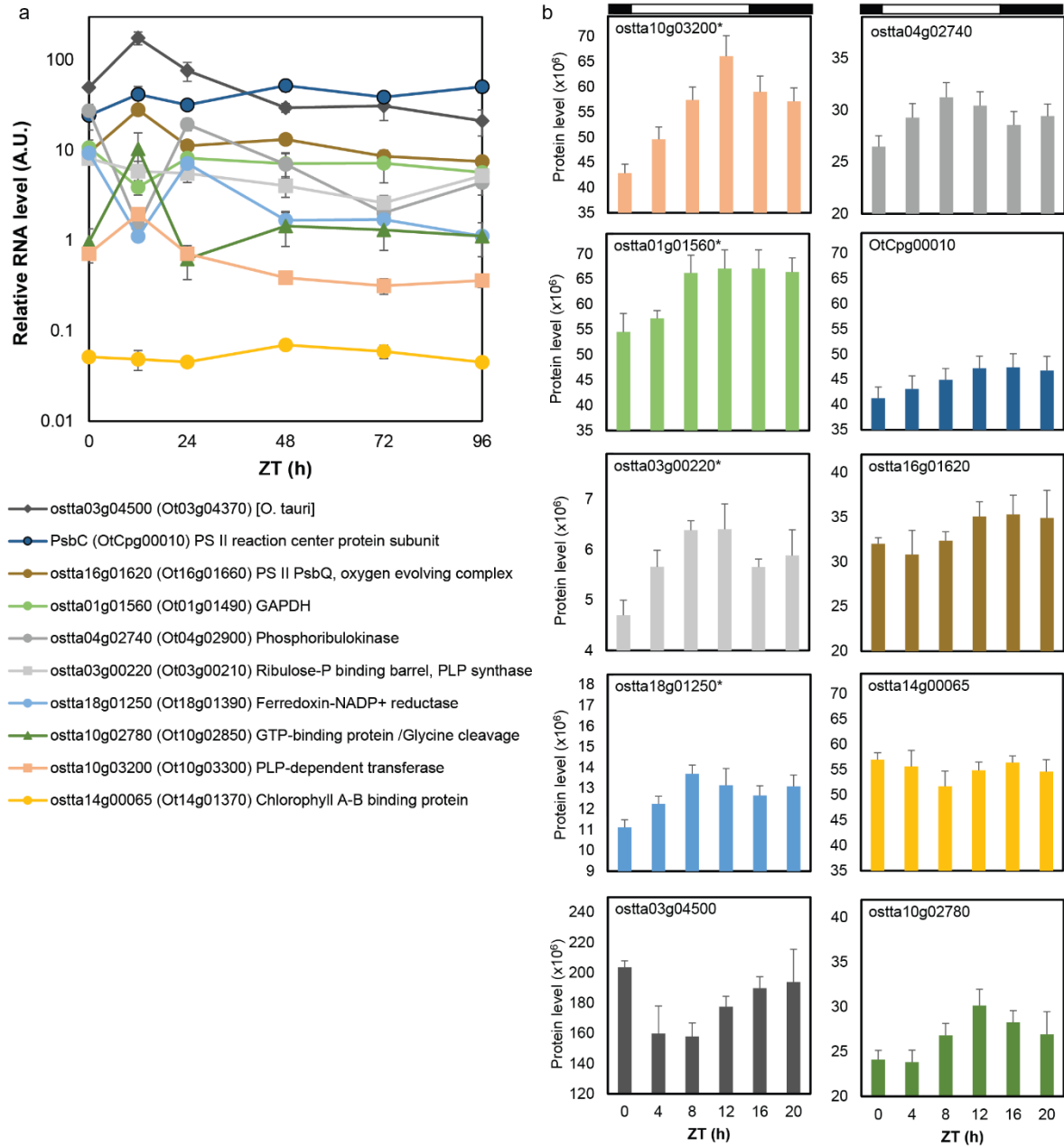
1221 **Supplementary Figure S7**

1222

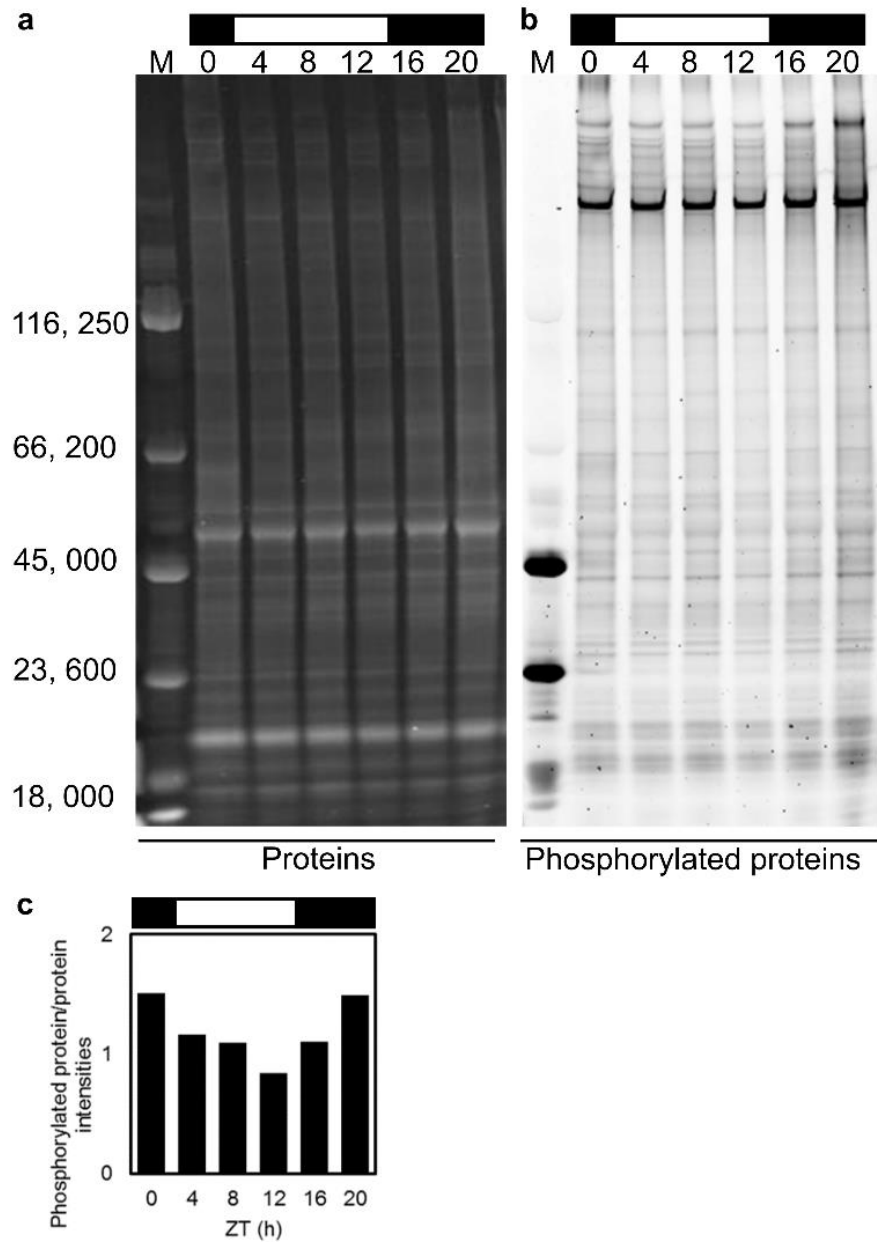


1223 **Supplementary Figure S8**

1224



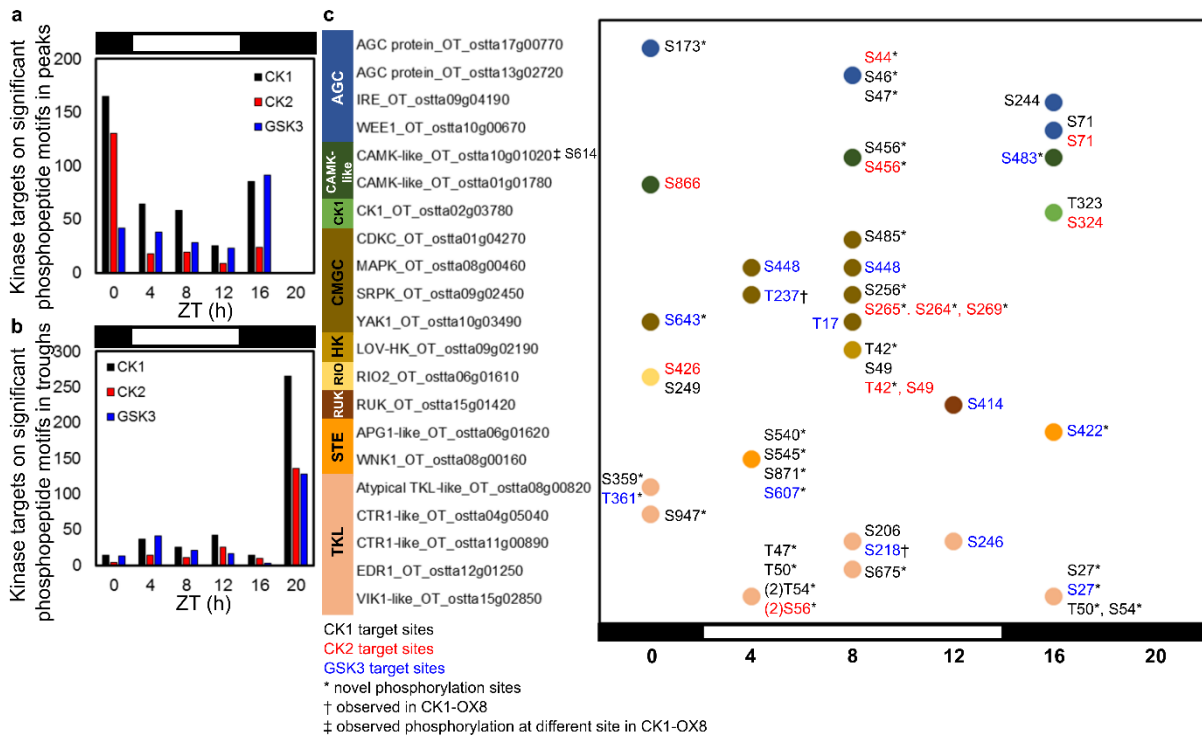
1225 **Supplementary Figure S9**



1226 **Supplementary Figure S10**

1227

1228



1229 **Supplementary Figure S11**

